REVIEW ARTICLE

Optical properties of gyroid structured materials: from photonic crystals to metamaterials

James A. Dolan[1,2,3]**, Bodo D. Wilts**[2,4]**, Silvia Vignolini**[5]**, Jeremy J. Baumberg**[3]**, Ullrich Steiner**[2,4] **and Timothy D. Wilkinson**[1]

[1] Department of Engineering, University of Cambridge, JJ Thomson Avenue, CB3 0FA, Cambridge, United Kingdom
[2] Cavendish Laboratory, Department of Physics, University of Cambridge, JJ Thomson Avenue, CB3 0HE, Cambridge, United Kingdom
[3] NanoPhotonics Centre, Cavendish Laboratory, Department of Physics, University of Cambridge, JJ Thomson Avenue, CB3 0HE, Cambridge, United Kingdom
[4] Adolphe Merkle Institute, University of Fribourg, Chemin des Verdiers 4, CH-1700 Fribourg, Switzerland
[5] Department of Chemistry, University of Cambridge, Lensfield Road, CB2 1EW, Cambridge, United Kingdom

E-mail: jad67@cam.ac.uk; bodo.wilts@unifr.ch; sv319@cam.ac.uk; jjb12@cam.ac.uk; ullrich.steiner@unifr.ch; tdw13@cam.ac.uk

Abstract. The gyroid is a continuous and triply periodic cubic morphology which possesses a constant mean curvature surface across a range of volumetric fill fractions. Found in a variety of natural and synthetic systems which form through self-assembly, from butterfly wing scales to block copolymers, the gyroid also exhibits an inherent chirality not observed in any other similar morphologies. These unique geometrical properties impart to gyroid structured materials a host of interesting optical properties. Depending on the length scale on which the constituent materials are organised, these properties arise from starkly different physical mechanisms (such as a complete photonic band gap for photonic crystals and a greatly depressed plasma frequency for optical metamaterials). This article reviews the theoretical predictions and experimental observations of the optical properties of two fundamental classes of gyroid structured materials: photonic crystals (wavelength scale) and metamaterials (sub-wavelength scale).

Keywords: gyroid, morphology, photonic bandgap materials, metamaterials

1. Introduction

The optical properties of matter are intrinsically linked to morphology. It is the vast range of possible morphologies and their characteristic length scales which give rise to the great wealth of optical phenomena we observe. At the atomic length scale, the amorphous or crystalline arrangement of atoms and their associated electronic interactions give rise to the refractive index of a material and determine the existence and nature of the electronic band gap and the associated optical transitions [1]. Significantly larger than the atomic length scale but still below the length scale of visible light, one can define and arrange synthetic "meta-atoms" or "meta-molecules". From these it is possible to construct a "metamaterial", an artificially engineered material designed to posses chosen electromagnetic properties not otherwise found in nature [2–4]. At the length scale of visible light, constructive and destructive interference resulting from cumulative interfacial reflections within a material give rise to photonic crystal effects and the associated photonic band gaps [5–8]. When considering the optical properties of a particular topological arrangement of matter it is clear that it is not just morphology but also the absolute length scale which is of importance.

Discovered in 1970 by Alan Schoen [9,10], the "Schoen G" or "gyroid" surface is a triply periodic minimal surface and therefore possesses a constant mean curvature (CMC) of zero and is periodic in all three principal spatial directions [11]. The gyroid surface possesses no reflection symmetries and exhibits an array of continuous channels along different principal crystallographic axes [12]. Its name derives from the observation that each continuous channel in the structure has connections to additional intersecting channels which "gyrate" along the channel length. These channels join as triads throughout the overall structure [13–15]. Closely related to and derived from the gyroid surface are the single and double gyroid morphologies. The unique geometrical properties exhibited by the gyroid surface and its related morphologies ensure gyroid structured materials are a particularly fascinating case study of the complex relationship between morphology and optical properties. Indeed, it is therefore unsurprising that such a rich variety of optical phenomena, from linear and circular dichroism to the recent prediction of Weyl points and line nodes, should derive from such materials [16,17]. The gyroid therefore stands apart from the otherwise diverse palette of structures similarly observed in nature.

This review details the theoretical and experimental investigation of the optical properties imparted to materials structured with the gyroid morphology. As the physical mechanisms responsible for the optical properties of these materials are distinguished primarily by the length scale on which the constituent materials are structured, two distinct classes of gyroid structured materials are considered: photonic crystals and optical metamaterials. After defining carefully the geometrical properties of the gyroid and describing its most convenient mathematical realisation (Sect. 1.1) the introduction concludes by presenting the basics of block copolymer self-assembly as a particularly promising means by which to fabricate both photonic crystal and optical metamaterial

gyroids (Sect. 1.2). The remainder of the article then examines the theoretical (Sect. 2.1) and experimental (Sect. 2.2) optical properties of visible wavelength scale gyroid photonic crystals, and again on the sub-wavelength scale the experimental (Sect. 3.1) and theoretical (Sect. 3.2) properties of gyroid optical metamaterials. Finally, the article concludes and offers an outlook to the potential directions for future optical research (Sect. 4).

1.1. Gyroid geometry and mathematical representation

Before presenting the anticipated and observed optical properties of gyroid structured materials, it is necessary to define more carefully the various gyroid morphologies, elucidate their relationship to the fundamental gyroid surface, and present their most convenient mathematical representation.

Although a precise analytical expression for the gyroid surface exists (see e.g. [12, 18]), it is convenient for purposes of clarity and efficient modelling to approximate its form through a level surface. These are defined by functions of the form $F : R^3 \to R$ and expressed as

$$F(x, y, z) = t, \tag{1}$$

where F determines the form of the surface via a space-dividing function and t is a constant which determines the volume fractions of the divided space.

Substitution of the lowest allowed Miller indices for the structure with space group $I4_132$ into the appropriate form of function F and setting the parameter t to zero results in the level surface approximation of the gyroid surface

$$\sin(\tilde{x}) \cos(\tilde{y}) + \sin(\tilde{y}) \cos(\tilde{z}) + \sin(\tilde{z}) \cos(\tilde{x}) = 0, \tag{2}$$

where $\tilde{x}$, $\tilde{y}$, and $\tilde{z}$ are scaled spatial ordinates such that $\tilde{x} = 2\pi x/a$, $\tilde{y} = 2\pi y/a$, and $\tilde{z} = 2\pi z/a$. The variable a is the cubic unit cell edge length. For a more detailed derivation see e.g. [12]. Although both the true gyroid surface and its level surface approximation are CMC surfaces, the former possesses zero mean curvature at every point of the structure and the latter a small non-zero curvature (Fig. 1). This approximate surface divides space into two sub-volumes of equal volume fraction and opposite handedness. The sub-volume on either side of the level surface has a morphology referred to as the "single gyroid".

Setting the parameter t to $0 < |t| \leq 1.413$ results in the level surface approximation of the single gyroid

$$\sin(\tilde{x}) \cos(\tilde{y}) + \sin(\tilde{y}) \cos(\tilde{z}) + \sin(\tilde{z}) \cos(\tilde{x}) = t, \tag{3}$$

which exhibits increased absolute mean curvature and which now divides space into two sub-volumes (single gyroids) of unequal volume fraction (Fig. 2a). The coupled increase and decrease of the two sub-volumes, the increase in absolute mean curvature of the dividing surface, and the offset of the new level surface from the $t = 0$ surface are all monotonic with increasing $|t|$ [19]. At $|t| = 1.413$ one of the two sub-volumes is no
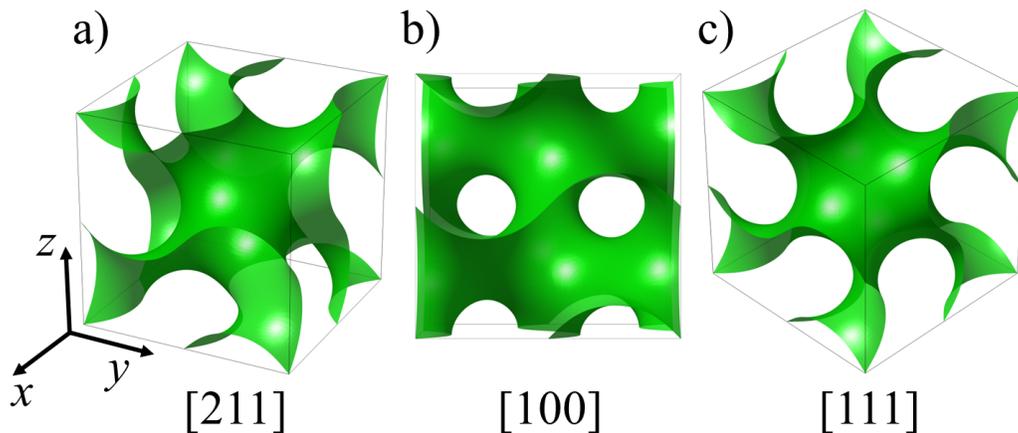
Figure 1. The gyroid surface morphology. a – c) Level surface approximation of the zero mean curvature gyroid surface (one unit cell) as defined by Eq. 2. The surfaces are viewed along the following crystallographic directions a) [211], b) [100], and c) [111].

longer continuous, referred to as the "pinch-off" of the level surface. Discontinuity of one of the sub-volumes persists in the range $1.413 < |t| \leq 1.5$, the morphology then having a body-centred cubic symmetry. For values of $|t| > 1.5$, the single gyroid level surface is no longer mathematically defined.

The single gyroid is unique amongst similar morphologies based on cubic minimal surfaces in that it is inherently chiral (i.e. its mirror image cannot be transformed to coincide with itself by translation and rotation) [20, 21]. Indeed, by joining the centrelines of the gyroid to create a periodic graph ("srs-net") one can readily identify local helices along the various screw axes of the gyroid [20]. For each of the [100], [111] and [110] directions, two screw axes can be identified and the associated helices exhibit opposing handedness and different average radii (Fig. 2b – d). For example, note that the [100] direction possesses local right-handed (left-handed) helical elements with a large (small) average radius, whereas the [110] direction possess local right- and left-handed helical elements of similar average radius. Though chirality is a symmetry property of the overall structure, it will be seen that the above considerations impart a strong anisotropy to the chiro-optic properties of any gyroid structured material.

Whereas the single gyroid level surfaces divide space into only two sub-volumes, a further simple alteration to the level surface equation allows the space to be divided into three continuous sub-volumes. By defining simultaneously both a positive and negative value of t, the level surfaces

$$\sin(\tilde{x})\cos(\tilde{y}) + \sin(\tilde{y})\cos(\tilde{z}) + \sin(\tilde{z})\cos(\tilde{x}) = \pm t \tag{4}$$

$(0 < |t| \leq 1.413)$ result in two interpenetrating single gyroid networks of equal volume fraction but opposite handedness, together forming the so-called "double gyroid" with space group $Ia\bar{3}d$ (Fig. 3). This is equivalent to the $t = 0$ surface with a finite thickness, which may be referred to as either the "matrix" or "majority" phase that separates the
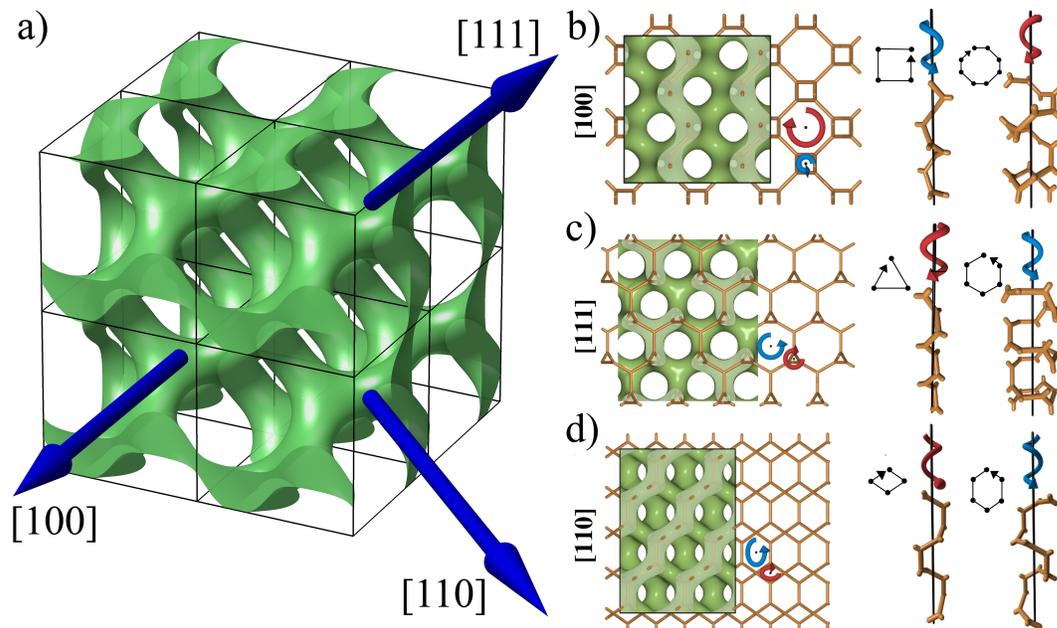
Figure 2. The single gyroid morphology. a) Level surface approximation of the single gyroid (eight unit cells arranged $2 \times 2 \times 2$) as defined by Eq. 3 with $t = 0.9$ (roughly 20% fill fraction). b – d) Projection along the crystallographic directions (high-symmetry directions) [100] (H), [111] (P), and [110] (N) of the single gyroid level surface and its "srs-net" (orange) highlighting the screw axes and their cross-sections. A left-handed local helical element is indicated by a blue arrow; a right-handed helical element by a red arrow. (b-d) used with permission from [20].

two single gyroid networks. As $|t|$ increases so does the volume fraction of the matrix phase.

One class of physical systems in which the gyroid morphology are exhibited are block copolymers. Due to the potential for such systems to self-assemble across a range of length scales and thereby act as a means of fabricating both photonic crystal and optical metamaterial gyroid structures, they are given particular attention before proceeding to discuss the optical properties of the resulting materials.

1.2. Block copolymer self-assembly

As will become clear throughout this review, the self-assembly of block copolymers is a particularly promising fabrication route for both gyroid structured photonic crystals and optical metamaterials. Self-assembly is the process by which a molecular system lowers its free energy by arranging itself into various patterns or structures. The basics of block copolymer self-assembly are therefore briefly covered here such that the specific fabrication methods and challenges associated with the two extremes of length scale may be discussed in more detail in the sections to follow. This brief introduction does not attempt to be comprehensive and for more thorough reviews on the topic see [11,22–29].

Block copolymers are covalently tethered homopolymers consisting of two or
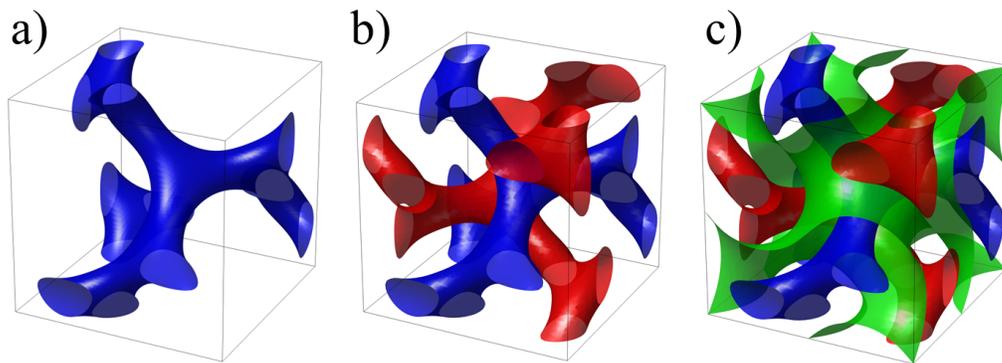
Figure 3. The double gyroid morphology. The level surface approximation (one unit cell) is defined by Eq. 4 with $t = 1.2$ (each single gyroid network roughly 10% fill fraction). a) The single gyroid structure ($t = 1.3$) without either the matrix phase or the second interpenetrating single gyroid phase. b) The double gyroid structure ($t = 1.3$) without the matrix phase as represented by the $t = 0$ gyroid surface. c) The division of space into three continuous sub-volumes by the definition of $t \to \pm t$ where the matrix phase is centred on the gyroid surface ($t = 0$) and fills the void between the two single gyroid networks.

more chemically distinct blocks (Fig. 4a – d). Linear block copolymers consist of such homopolymers arranged in a non-repeating fashion (e.g. ABC, where each letter represents a different homopolymer). The simplest block copolymer system is the linear AB diblock copolymer and its phase behaviour captures the essential elements of the behaviours of more complex block copolymers (e.g. linear triblock terpolymers). The bulk thermodynamic equilibrium morphology of a diblock copolymer depends on three parameters: N, the total degree of polymerisation; f_A or f_B, the volume fractions of homopolymer A or B respectively ($f_A + f_B = 1$); and χ, the Flory-Huggins interaction parameter specific to the chemical properties of the two homopolymers (a measure of the repulsion of the monomers). The interaction parameter χ is generally small and, for copolymers without strong specific interactions (e.g. hydrogen bonds), varies inversely with temperature. It is the product χN which determines the equilibrium morphology of the diblock copolymer of a particular composition at a given temperature. The theoretical phase diagram for such a copolymer shows the expected equilibrium morphologies (Figs. 4e and 5). As long as the enthalpic interaction between the blocks (χ) or the total molecular weight of the copolymer (N) are sufficiently large (i.e. the total enthalpic interaction between the blocks is sufficiently unfavourable), the copolymer is in the strong segregation limit ($\chi N \gg 10$). The equilibrium morphology minimises the overall free energy of the system by balancing the enthalpic (interfacial) and entropic (chain stretching) energy contributions. The morphology of interest here, that of the double gyroid, is found within a narrow compositional window (i.e. range of values for f_A or f_B) between hexagonally packed cylinders and lamellae.

Although a particular morphology may well be a thermodynamic minimum of the free energy of the bulk system, two additional effects can prevent the formation of
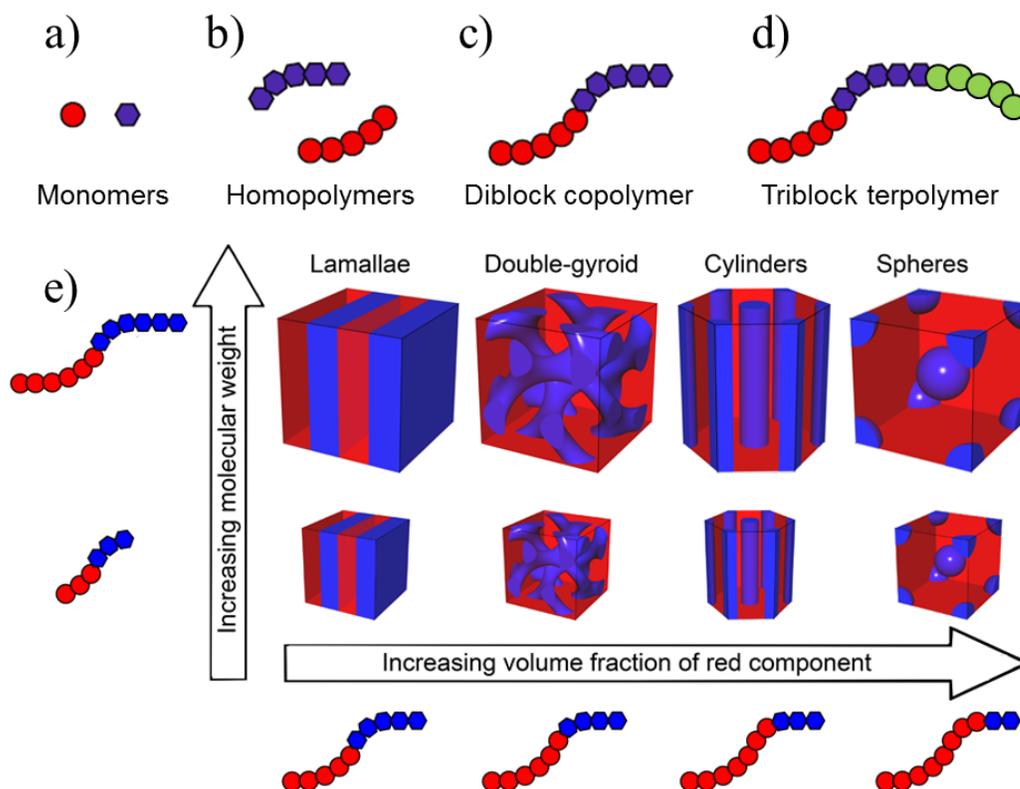
Figure 4. Block copolymers and self-assembled equilibrium morphologies. a) Two chemically distinct monomer species. b) Homopolymers composed of the two chemically distinct monomers. c) Linear diblock copolymer in which the two homopolymers are covalently tethered. d) Linear triblock terpolymer in which the three homopolymers are covalently tethered. e) Equilibrium morphology and characteristic periodicity for a micro-phase separated diblock copolymer. The variation of the relative volume fraction of the two homopolymer blocks determines the equilibrium morphology adapted by the copolymer whereas variation in the overall molecular weight of the copolymer determines the periodicity of the resulting structure. Used with permission from [30].

this morphology. One effect is the kinetics of the self-assembly process. Whereas the periodicity of the block copolymer phase increases with increasing N (e.g. the spacing of layers in lamellae forming diblock copolymers scales as $N^{2/3}$) the rate of diffusion of polymer chains within the system decreases exponentially with increasing N (i.e. diffusion $D \sim e^{-N}$). It is therefore possible that the self-assembly process takes place over a prohibitively long time. Alternatively, the copolymer may become trapped in a metastable state (e.g. the hexagonally perforated lamellar phase) due to finite kinetic barriers [32, 33]. Similarly, the kinetic penalties of reorienting variously oriented microdomains (grains) to create a minimum free energy structure with long range order may be prohibitively large given the low rate of diffusion of the polymer chains. It is therefore anticipated that the size of the microdomains will vary inversely with the long range order of the system. A common means to increase the rate of diffusion within the system (i.e. to reduce its viscosity) is to swell the copolymer with a low molecular
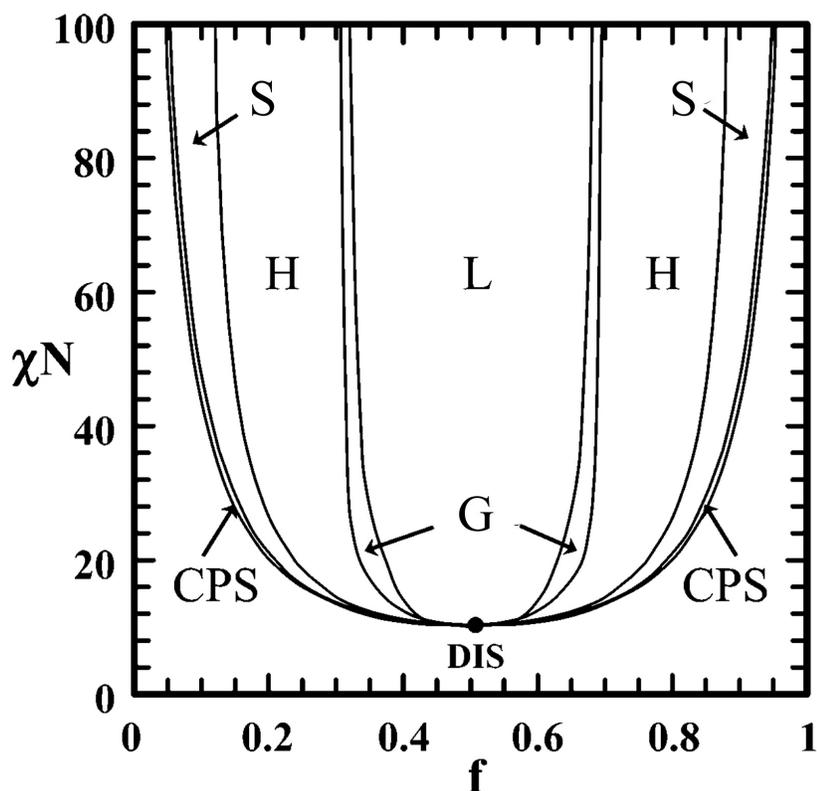
Figure 5. Theoretical phase diagram for a linear diblock copolymer. The product χN determines the equilibrium morphology of the micro-phase separated system for a particular composition of copolymer, where χ is the Flory-Huggins interaction parameter between the two blocks and N the total degree of polymerisation of the copolymer. The parameter f is the fill fraction of one or other of the two blocks (i.e. f_A or f_B). The various equilibrium morphologies which minimise the thermodynamic free energy of the segregated system are: lamellae (L), the double gyroid (G), hexagonally packed cylinders (H), body-centred cubic packed spheres (S), and close-packed spheres (CPS). Otherwise the system is disordered (DIS). Reprinted with permission from [31]. Copyright 2006 American Chemical Society.

weight organic solvent. However, assuming that none of the blocks are preferentially soluble in the solvent (i.e. that the solvent is "neutral") and that the phase diagram of the system is therefore unchanged, the solvent lowers the effective χ-value, and various additional kinetic factors, such as the rate of evaporation of the solvent, may alter the resulting morphology.

The second effect which may prevent the self-assembly of a block copolymer into its bulk thermodynamic equilibrium morphology are interfacial and commensurability considerations which dominate the behaviour of polymer thin films. For example, any difference in surface energy of the various blocks of the copolymer at either the substrate-polymer or polymer-air interfaces (which might also depend on the nature and concentration of any solvent present) may lead to preferential wetting of one block of the copolymer at the interface. Any morphology thus imposed by the interfaces

(e.g. lamellae aligned parallel to the substrate) will persist for a finite distance into the copolymer film which, if the film is sufficiently thin, may be its entire thickness. Also, should the total thickness of the copolymer film be incommensurate with the characteristic periodicity of the equilibrium morphology then either the morphology or its orientation may alter to accommodate imposed boundary conditions.

In the following sections we review how gyroid structured materials, which may be fabricated (amongst other methods) using block copolymer self-assembly, interact with visible light both in theory and experiment. Firstly, on a length scale of the order of visible light, where gyroid structures may act as photonic crystals, and secondly on a smaller sub-visible light length scale, such that the material exhibits a characteristic metamaterial response.

2. Gyroids on the wavelength scale: photonic crystals

Photonic crystals are materials in which the refractive index varies periodically in one, two or three dimensions, and for which the characteristic length scale of such variations is comparable to the wavelength of visible light [8,34–36]. The role of this periodic variation in refractive index for the propagation of light is analogous to a periodic variation in potential for an electron propagating through a semiconductor crystal. Whereas the crystal lattice of the semiconductor affects the existence and properties of its electronic band gap, the manner in which the refractive index is varied spatially in a photonic crystal determines the existence and properties of the optical equivalent, the photonic band gap.

A photonic band gap is a range of frequencies for which the propagation of light through the photonic crystal is forbidden and light of a wavelength within the band gap is therefore reflected from its surface or trapped within its interior [8]. Band gaps can be divided into two types: complete and partial. When propagation is inhibited for any direction or polarisation state of light the photonic band gap is defined as complete, while we define a partial band gap (or stop band) when the photonic crystal may allow light propagation in some directions or for certain polarisations.

Some optical applications require a band gap that is wide, robust and complete over the desired spectral range [6, 8] and, practically, should extend over a large area with long range order [37, 38]. Photonic crystals, and especially those with a complete band gap, have numerous potential applications, aimed at optical circuitery by guiding light controlled through defined defects [39, 40], manipulating the local density of states to inhibit spontaneous emission of internalised fluorophores [41–43] or interference-based reflectors [8].

2.1. Theoretical predictions of gyroid photonic crystals

The basic requirement for a dielectric network structure to exhibit a photonic band gap is the modulation of the dielectric constant (i.e. the refractive index) along a particular

direction. If sufficient dielectric modulation exists in all three principal directions, and the symmetry of the structure is high, a complete photonic band gap may be achieved [8]. These conditions may be satisfied by a structure with reciprocal lattice vectors for the dielectric modulations which are as equal as possible (i.e. a structure with an approximately spherical Brillouin zone). Both the single gyroid and the single diamond structures are excellent examples of such a structure [6]. Also cubic symmetry, found in both these structures, ensures that the optical properties are identical along any set of three orthogonal directions [11, 12, 44].

2.1.1. Gyroid photonic band gap Theoretical investigation of the photonic band gap properties of the various gyroid structures is most immediately carried out by calculation of the photonic band structure. Starting in 1999 with Martin-Moreno *et al.* numerous authors have investigated the photonic band gaps of not only the gyroid but also the cubic and diamond minimal surface morphologies and other triply periodic bicontinuous cubic structures [11–14, 38, 45–51]. Finite-difference time-domain (FDTD) simulations [45, 48, 52] and plane wave expansion methods [14, 38, 46, 47] have proved to be the two main simulation methods to investigate the photonic band gap of these triply periodic cubic structures. It should be noted that the latter theory is only exact for ideal and infinite photonic crystals, while FDTD modelling allows the simulation of arbitrary geometries and defects [53–55]. However, apart from small deviations due to methodology, all results agree well across different theoretical studies and with experimental results.

Fig. 6 plots the photonic band gap of a single gyroid photonic crystal along the high-symmetry points of the associated Brillouin zone. As can be seen, the gyroid photonic crystal may exhibit a complete and sizeable photonic band gap (dielectric contrast of 13 and fill fraction of roughly 30%). In addition, it is clear from the band structure that the reflectance and transmission spectra of the gyroid photonic crystal vary significantly depending on the relative orientation of the crystal and the incoming light (Fig. 7a) [50, 52, 56]. Michielsen *et al.* in 2010 investigated the reflectivity of the gyroid photonic crystal cut along fourteen different planes (incident light perpendicular to the cut plane) to demonstrate this shift in the reflectivity maxima from the ultraviolet to the green-yellow wavelength range (363 nm unit cell size at a fill fraction of 17% and a high-ε phase with refractive index $1.56 + i0.06$; see Fig. 7b) [52].

According to Maldovan *et al.* in 2004, all structures exhibiting a large (complete) photonic band gap, such as the gyroid, are based on diamond-like networks with a fill fraction (high-ε phase) of roughly 20% [6]. Remarkably, even considerable modification of the structure, i.e. randomisation and other imperfections, does not necessarily destroy the photonic band gap, although it does strongly reduce its width [57, 58]. This robustness to structural alterations allows the identification of approximate structures which may be simpler to fabricate (e.g. the woodpile photonic crystal [6, 8]).
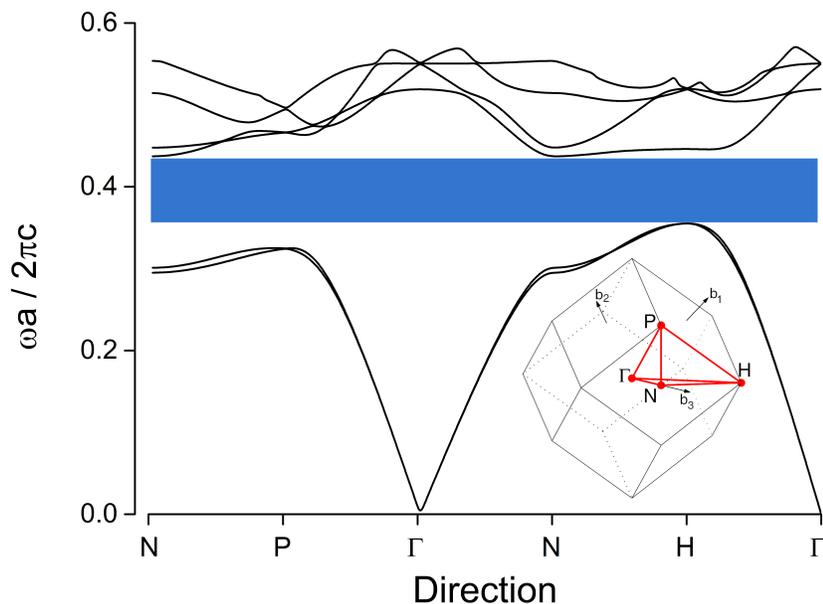
Figure 6. Photonic band diagram of a single gyroid photonic crystal. The dielectric contrast is 13 (e.g. silicon and air) and the fill fraction is roughly 30%. The parameter $\omega a/2\pi c = \tilde{\omega}$ refers to the normalised frequency where ω is the frequency of the incident light, a is the unit cell size and c is the speed of light in vacuum. The complete photonic band gap is highlighted in blue. The inset shows the first Brillouin zone of the gyroid topology having body-centred cubic symmetry, the high-symmetry points N, P and H (see Fig. 2), and reciprocal lattice vectors $\vec{b}_i$. The central point of the first Brillouin zone is labelled Γ.

2.1.2. Effect of structural and material parameters on the gyroid photonic band gap The optical properties of a gyroid photonic crystal can be characterised by the bandwidth and mid-gap frequency of the photonic band gap. These vary according to the unit cell size, dielectric contrast and fill fraction of the structure [6, 8, 45, 59]. Following the terminology often adopted in the literature, the band gap "quality" (i.e. the relative size of the band gap) is defined as the percentage ratio of the band width to the mid-gap frequency $\Delta\omega/\omega_0$; the dielectric contrast is defined as the ratio of the dielectric constant of the high-ε phase to that of the low-ε phase of the network; and the fill fraction is defined as the volume percentage occupied by the high-ε phase. A photonic band gap only exists for a judicious choice of the above parameters. We will first present the influence of each parameter in detail before showing experimental validation.

Unit cell size. Due to the scaling properties of Maxwell's equations and the relative invariance of many dielectrics' permittivity with frequency [1], the theoretical results thus far derived are applicable to purely dielectric photonic crystals of any lattice size. Indeed, Pouya *et al.* in 2012 took advantage of this scaling invariance to study gyroid photonic crystals via a macroscopic polymer replica operating in the microwave regime [60]. Unit cell size may therefore be explicitly accounted for in the theoretical calculation of photonic band gap by calculating the normalised rather than the absolute
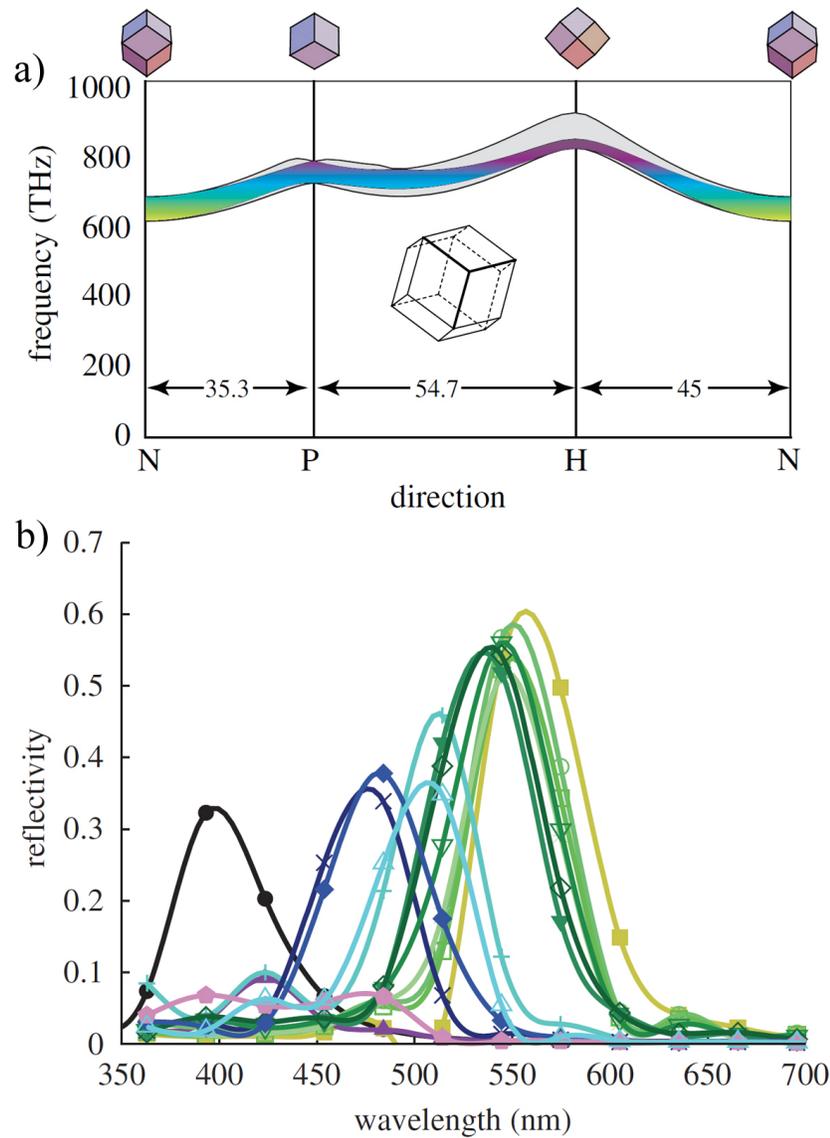
Figure 7. Angular dependence of the optical properties of a single gyroid photonic crystal. a) The band photonic diagram for a single gyroid with a fill fraction of 50% and a refractive index contrast of 1.5 which exhibits only partial band gaps. The arrows between the high-symmetry points indicate the (shortest) spatial angle between these points. The inset shows the first Brillouin zone (compare Fig. 6). Copyright ©2009, The Royal Society. b) Explicit FDTD calculations of reflectivity spectra for various orientations of a single gyroid with a fill fraction of 17%, a refractive index contrast of 1.56+i0.06 and a unit cell size of 363 nm. The incident light has transverse polarisation. The different domain orientations are characterised by their Miller indices (hkl); each curve corresponds to a different orientation. Used with permission from [52].

frequency. Normalised frequency is defined as $\omega a/2\pi c = \tilde{\omega}$, where ω is angular frequency, a is the cubic lattice constant, and c is the speed of light in vacuum. It may therefore be seen that the photonic band gap $\Delta\omega$ is inversely proportional to the lattice constant. As an example, at an optimal fill fraction of 17% and for a dielectric contrast of 13, the normalised band gap $\Delta\tilde{\omega}$ of a gyroid photonic crystal was calculated by Maldovan *et al.* in 2002 ranging from 0.421 to 0.540 [47]. The wavelength λ_0 associated with the mid-gap frequency is $\lambda_0 = a/\tilde{\omega}_0$, where $\tilde{\omega}_0$ is in units of normalised frequency. As the mid-gap frequency of the complete gap tends to lie in the range $0.4 - 0.6$ (depending on dielectric contrast and fill fraction as explored below) the mid-gap wavelength may be approximated as roughly twice the lattice constant ($\lambda_0 \approx 2a$). Photonic band gaps in the optical regime, i.e. in the range of 400-700 nm, are therefore expected for gyroids with a lattice constant on the order of 200-350 nm [13–15, 45, 56].

Dielectric contrast. Without a sufficient dielectric contrast between the high-ε and low-ε phases of a photonic crystal no complete band gap opens up [8, 50, 61]. There is therefore a minimum dielectric contrast, different for each photonic crystal morphology, below which the complete band gap is closed and above which the band gap width increases with increasing dielectric contrast [59]. The crystal morphology which, for a given unit cell size and fill fraction, has the lowest minimum dielectric contrast required for a complete band gap is often referred to as a "champion" structure. A champion photonic crystal will therefore possess the largest band gap for a given dielectric contrast and (optimised) fill fraction.

Martin-Moreno *et al.* in 1999 first calculated the variation of the band structure of the gyroid photonic crystal with dielectric contrast [45]. Investigating various triply periodic morphologies with a fill fraction of 50% and a dielectric contrast of 13 (that of silicon), the authors identified a complete band gap for both the gyroid and double diamond structures. Further investigating the effect of dielectric contrast upon the gap quality, it was demonstrated that a minimum dielectric contrast of ∼6.25 is required to open a complete band gap for a gyroid structure, and that the quality of this gap increases to ∼12% for a contrast of 36, highlighting the need for a large dielectric contrast. This compares to a minimum dielectric contrast of only ∼4 to open a complete band gap for a double diamond structure, which increases to ∼18% for a contrast of 36. Thus the diamond morphology is considered the champion photonic crystal with the gyroid a close second [6, 62]. Note however that the diamond structure does not exhibit the chirality of the gyroid.

These initial theoretical results were confirmed thereafter by a number of authors. Babin *et al.* in 2002 explored the band structures of single gyroid photonic crystals (as well as hollow and double gyroid structures) and investigated the effect upon the photonic band gap of a varying dielectric contrast for a single gyroid structure at 18.5% fill fraction (Fig. 8a and c) [46]. For this improved fill fraction, a lower minimum dielectric contrast of 5 was required to open a complete band gap and a gap quality of over 25% could be achieved at a dielectric contrast of 13. Similarly, Maldovan *et*

al. in 2002 investigated the single gyroid structure at a fill fraction of both 50% and 17%, and found minimum dielectric contrasts for a complete band gap of 7 and 5.2 respectively [47]. Note also from Fig. 8a and c that the mid-gap frequency can be seen to monotonically decrease with dielectric contrast once a complete gap has opened.

Fill fraction. As intimated above, a careful choice of the fill fraction of the high-ε phase of the gyroid photonic crystal can lead to an optimal band gap quality for a given dielectric contrast. Babin *et al.* in 2002 first studied the effect of fill fraction on the band gap quality (Fig. 8b and d) [46]. For a single gyroid with a dielectric contrast of 13, a maximum band gap quality of 26.6% was calculated at a fill fraction of 19%. The mid-gap frequency ω_0 was predicted to decrease monotonically with fill fraction when a complete band gap exists.
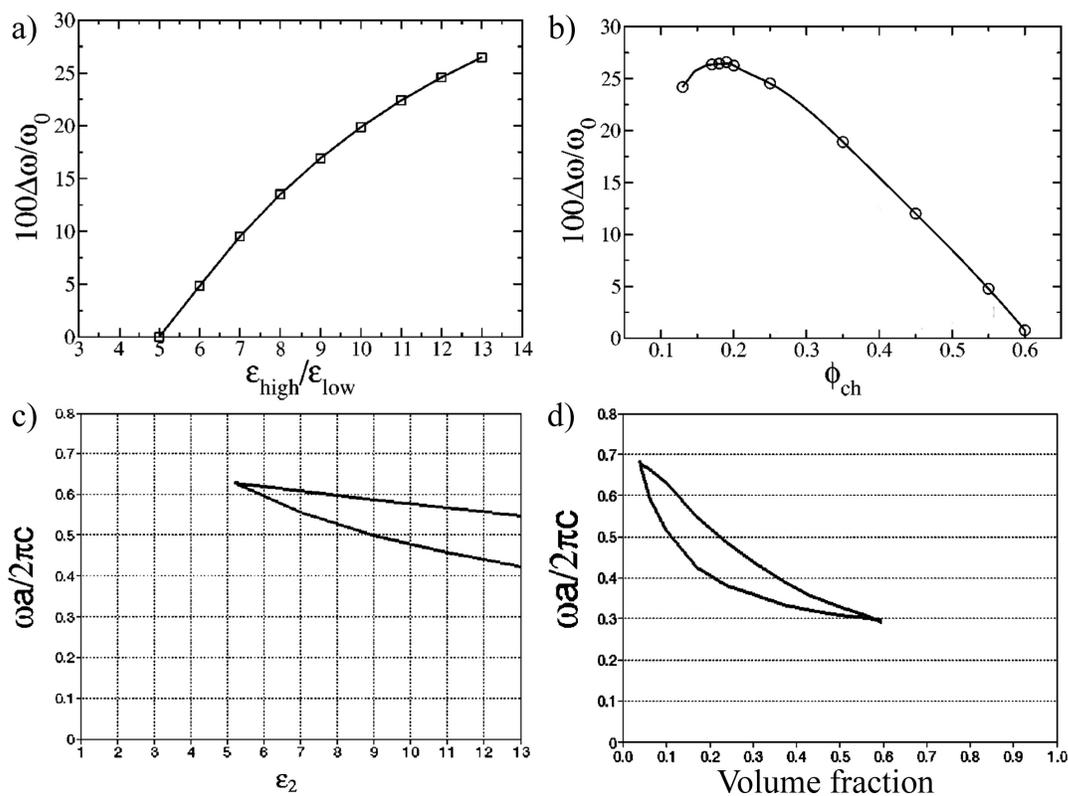
Figure 8. Dependence on structural properties of the photonic band gap of single gyroid photonic crystals (i.e. band gap maps). a) Variation of normalised band gap quality ($\Delta\tilde{\omega}/\tilde{\omega}_0$) with dielectric contrast ($\varepsilon_{high}/\varepsilon_{low}$) for a single gyroid with a fill fraction of 18.5%. b) Variation of normalised band gap quality with fill fraction (ϕ_{ch}) for a single gyroid with a dielectric contrast of 13 (e.g. air and silicon). c) Variation of the band edges (and therefore mid-gap frequency) with dielectric contrast (ε_2) for a single gyroid with a fill fraction of 17%. d) Variation of the band edges with fill (volume) fraction for a single gyroid with a dielectric contrast of 13. Adapted from [46].

Table 1. Effect of increase in various material parameters upon the normalised band gap quality ($\Delta\tilde{\omega}/\tilde{\omega}_0$) and mid-gap frequency ($\tilde{\omega}_0$) of single gyroid photonic crystals, where $\tilde{\omega}$ is the normalised frequency $\omega a/2\pi c$. $\uparrow$ indicates a proportional relationship, $\downarrow$ an inverse relationship, $\updownarrow$ that there is an optimum value, and "–" that the parameters are independent. Note that the relationships are valid only for a parameter combination for which a complete band gap exists.

	$\Delta\tilde{\omega}/\tilde{\omega}_0$	$\tilde{\omega}_0$
Dielectric contrast ($\varepsilon_{\text{high}}/\varepsilon_{\text{low}}$)	$\uparrow$	$\downarrow$
Volumetric fill fraction (ϕ)	$\updownarrow$	$\downarrow$
Unit cell size (a)	–	$\uparrow$

Summary. The effect of dielectric contrast, volumetric fill fraction and unit cell size on the band gap quality and mid-gap frequency for a single gyroid photonic crystal are summarised in Table 1. It is clear that in order to achieve a complete photonic band gap the dielectric contrast must be as large as practicably achievable and the fill fraction of the high-ε phase must be carefully tuned (to a value close to 20%). The mid-gap frequency of the photonic band gap is then determined primarily by the periodicity of the structure (i.e. the unit cell size) and is decreased by both increased dielectric contrast and fill fraction.

2.1.3. Polarisation dependent optical properties The variation in the optical properties of a gyroid photonic crystal with the polarisation state of the incident light, including optical activity and dichroism, have been noted by a number of authors. Michielsen *et al.* in 2010 described how gyroid photonic crystals could rotate the plane of linearly polarised light (optical activity), how the scattered intensity differed for transverse magnetic and transverse electric linear polarisations (linear dichroism), and how the scattered light was found to be elliptically polarised [52, 56].

However, the gyroid geometry possesses a unique property compared to other triply periodic constant mean curvature structures which attracts particular interest: it is intrinsically chiral and can thus potentially exhibit strong circular as well as linear dichroism [16, 63]. The helical nature of the high-ε phase is particularly evident when viewed along the [100] and [111] crystal axes (Fig. 2b – d) and the "strength" of the chirality is therefore strongly anisotropic [15, 16, 38]. It should be noted that although the symmetric double gyroid possesses two single gyroid networks, these are of opposite handedness and the overall structure is therefore achiral [18, 44]. However, an overall chirality can be induced in a double gyroid structure if the symmetry between the two high-ε phases is broken or if more than two networks are stacked [16, 18]. Note that such a structure is no longer strictly a double gyroid as previously defined.

The circular dichroism of the gyroid can therefore be analysed through an investigation of the propagation of circularly polarised light incident on the structure, as considered by Saba *et al.* in 2011 and 2014 (Fig. 9) [16, 20]. The authors identified a

clear circular polarisation band gap in the single gyroid (i.e. the lack of an appropriate circularly polarised band at the frequency of the incident light) for the [100] direction (Fig. 9). Circular dichroism is also expected, to a far lesser extent, in the [111] direction and not at all in the [110] direction (Fig. 9b), highlighting the strong anisotropy of any chiro-optic effect in the gyroid. Note that the circular polarisation band gap allows transmission of light with a circular polarisation of the same handedness as that of the dominant helical high-ε phase of the structure. Sufficient discrimination between circularly polarised light of different handedness by three-dimensional structures such as the gyroid opens the tantalising possibility of negative refraction without the requirement for a doubly negative material [44].
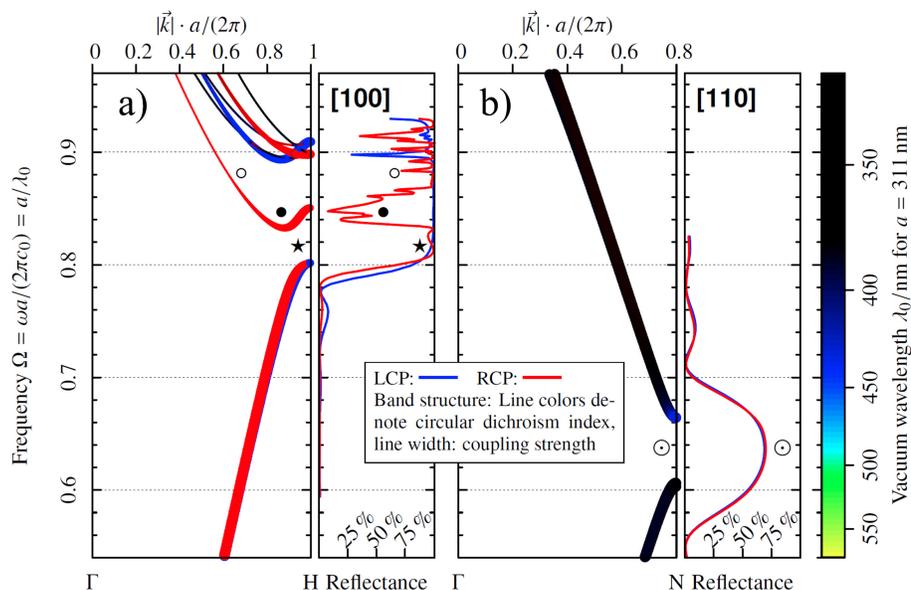
Figure 9. Circular dichroism of the single gyroid structure. a – b) Portion of the photonic band diagram (left) and simulated reflectance spectrum (right) for a single gyroid with fill fraction of 20% and a dielectric contrast of 2.4, where ω is the frequency of the incident circularly polarised light, λ_0 its wavelength, a is the unit cell size and c_0 is the speed of light in vacuum. The colour bar on the right shows the vacuum wavelength of visible light assuming a unit cell size of 311 nm. The circularly polarised light is incident either along the a) [100] or b) [110] direction. Along the [100] direction, there is a conventional band gap for unpolarised light ($\star$) and a circular dichroic band gap ($\bullet$) for left-circularly polarised light (i.e. circular dichroism). Along the [110] direction, only a conventional band gap ($\odot$) without circular dichroism is observed. Adapted with permission from [20].

2.1.4. Double gyroids and related photonic crystal morphologies Whereas a single gyroid photonic crystal possesses a wide and robust photonic band gap for a sufficiently large dielectric contrast, the double gyroid structure displays no such complete gap [6, 64]. Indeed, Maldovan *et al.* in 2002 were unable to identify any dielectric contrast within the range 1-20 (outside the range of most known materials at optical frequencies)

for which the structure displayed a complete gap [47]. However, as noted by Michielsen and Kole in 2003, the double gyroid structures previously studied comprised only of symmetric high-ε phases (i.e. both high-ε phases possessed the same fill fraction and dielectric permittivity) [48]. When the symmetry between the two high-ε phases is broken, e.g. by shifting the two single gyroid networks, a complete band gap can develop in the double gyroid structure [65]. Depending upon the degree of asymmetry the resulting band gap quality may be significantly reduced compared to the single gyroid structure [46]. It therefore seems that, for photonic crystal applications at least, the symmetric double gyroid structure is of only limited interest.

As commented upon by Babin *et al.* in 2002, triply periodic multicontinuous architectures such as the single gyroid have resulted in some of the widest complete photonic band gaps thus far investigated [46]. However, the authors' study of various 2-, 3-, 4- and 5-subvolume triply periodic structures (e.g. double and perforated networks) again yielded only weaker gaps as compared to the simpler single gyroid morphology. Further investigation of various multicontinuous structures by Michielsen *et al.* in 2003 highlighted again the general trend that cubic structures with simple topologies (lower genus, i.e. connectivity) exhibit complete photonic band gaps in a way which more complex structures (higher genus) do not [48]. Other photonic crystal morphologies of genus 3 with cubic symmetry exist, with the diamond phase possessing a Brillouin zone that closely resembles a sphere which makes it the champion structure for photonic crystal applications [47, 48, 50, 56]). The simple cubic structure is of less interest due to its relatively poor optical performance.

Clearly, the range of other more complicated structures based upon these fundamental morphologies is unlimited (e.g. intertwining multiple structures of similar type [16, 18, 66]). However, due to the difficulty of fabricating such complicated structures and their only limited appearance in nature [44, 67], they lie outside of the scope of this review.

2.2. Experimental observations of gyroid photonic crystals

Gyroid photonic crystals are predicted to exhibit a photonic band gap (either partial or complete, depending on the dielectric contrast and fill fraction), linear and circular dichroism, and optical activity. Experimental verification of these properties therefore relies upon ready access to appropriately sized dielectric gyroid structures. Fortunately, the gyroid is a morphology often found in natural and synthetic self-assembled systems. Butterfly wing scales and block copolymers thus offer two immediate means by which to experimentally explore the optical properties of gyroid structured materials. In addition, as so-called "top-down" assembly methods such as direct laser writing (see below) have continued to improve, yet another route to gyroid photonic crystals has become available. The measured optical properties of gyroids are therefore presented below according to the nature of the structure under study: biological gyroids, biotemplated gyroids, block copolymer gyroids, and gyroids assembled by top-down methods.

2.2.1. Biological gyroid structures The gyroid is one of the most complex of the mesoscopic self-assembled bicontinuous structures found in nature [13, 15, 21, 56, 60, 68]. Whereas 3D photonic crystals still present various challenges to artificial synthesis, nature provides a relative abundance evolved over millions of years [13, 14, 34, 38, 50, 51, 69–72]. Biological gyroid photonic crystals, repeatedly identified as a means of imparting structural colour in the wing scales of butterflies, therefore offer the most immediate and accessible experimental route to the investigation of the optical properties of the gyroid morphology (Fig. 10).
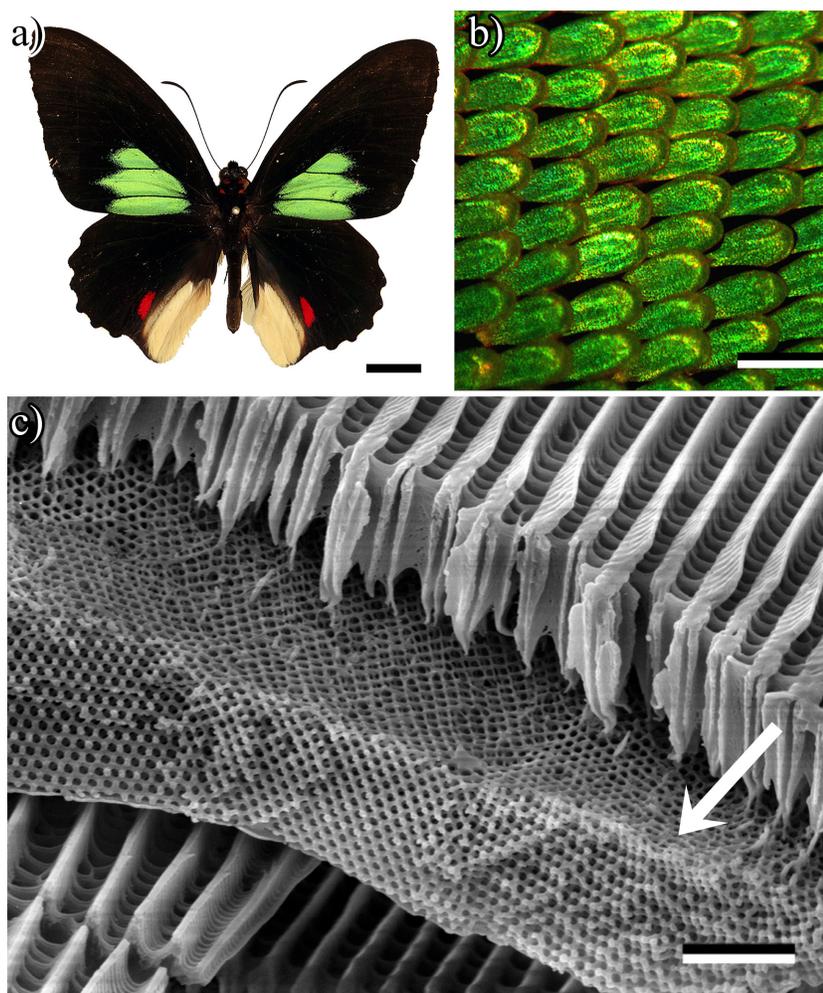
Figure 10. Biological gyroids, here in wing scales of the butterfly *Parides sesostris.* a) The butterfly (scale bar: 1 cm). b) The scales imbricating the wing (scale bar: 100 μm). c) An electron micrograph of a cross section of the wing scale showing the gyroid structure and also highlighting the ridge and cross-ribs present on top of the gyroid photonic crystal (scale bar: 2 μm).

Michielsen *et al.* in 2008 first positively identified the gyroid morphology in the wing scales of various papilionid (*Parides sesostris* and *Teinopalpus imperialis*) and lycaenid (*Callophrys rubi, Cyanophrys remus, Mitoura gryneus* and *Callophrys dumetorum*) butterflies [13, 14]. The authors used a combination of characterisation techniques (such

as scanning and transmission electron microscopy) and level-set modelling of different morphologies to resolve the previous uncertainty as to the identification of the structure. Such uncertainty arose quite understandably from the challenge of unambiguously distinguishing between various feasible morphologies given the necessarily random cross-sections, orientations and thicknesses of the samples under study. Further investigation into the structure of butterfly wing scales yielded similar results [14,38,56,73] such that, by 2011, all 3D photonic crystals found in butterfly wing scales had been positively identified as being of gyroid type.

Since the explicit identification of butterfly wing scale photonic crystals as gyroid, a number of authors have explored their optical properties (Fig. 11), the first being Michielsen *et al.* in 2010 [52]. Investigating the wing scales of *Callophrys rubi*, the authors determined the reflectivity spectra of a 363 nm unit cell gyroid photonic crystal with a fill fraction of 17% and noted its similarity to that of an oak leaf, which is important for biological reasons since it offers camouflage in a folicaeous habitat. Saranathan *et al.* in 2010 investigated the reflectivity of the wing scales of five papilionid and lycaenid butterflies with unit cell sizes ranging from 250 to 330 nm and chitin filling fractions from 25% to 34% [14]. Curiously, the wavelength of the resulting reflectance peak varied only from 545 to 550 nm despite the variation in structural parameters (see Table 1). More recently, Mille *et al.* in 2011 and 2013 again investigated the reflectivity of wing scales of *Callophrys rubi* with an estimated unit cell size of 339±5 and 336±3 nm respectively (fill fraction 30% and refractive index $1.55 + i0.06$) [51,73]. Note that whereas the reported fill fraction and the unit cell size of gyroid structures in butterfly wing scales can vary considerably, even within the same species of butterfly, the resulting green colouration is remarkably stable. These parameter variations may be natural (e.g. due to different developmental conditions) or arise by some other mechanism (e.g. a genetic mechanism controlling expression of chitin).
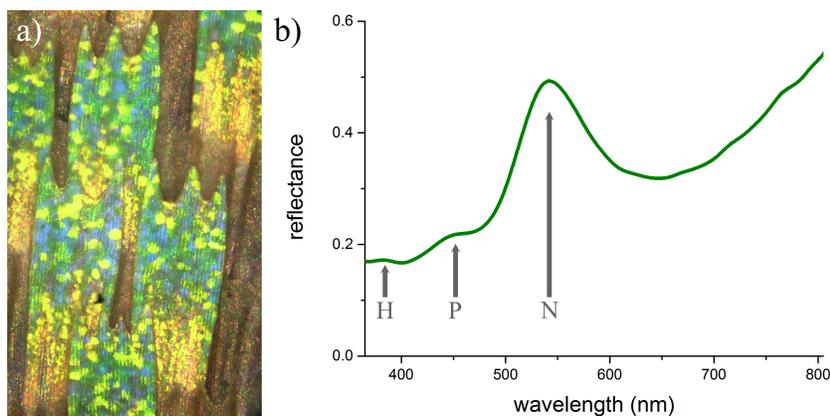
Figure 11. Reflectivity spectra of a biological gyroid. a) Optical micrograph of *Callophrys rubi* wing scales and b) their reflectivity spectra. The arrows label the high symmetry points of the structure and correspond to the approximate position of the (partial) photonic band gaps as highlighted in Fig. 6.

Where gyroid photonic crystals have been studied theoretically, an infinite or semi-

infinite perfect crystal is often assumed. However, butterfly wing scales are composed of numerous domains of gyroid photonic crystals, each oriented differently and therefore exhibiting a different optical response (e.g. peak reflectance) [20, 38, 51, 52, 74]. This polycrystallinity of the photonic crystal affects the overall optical properties of the wing scale, counterintuitively often imparting an angle-independent colour effect, which might be mistaken for a complete photonic band gap [13]. The fact that the band gap of such structures is not complete (due to the low dielectric contrast provided by the biopolymer chitin of which these structures are comprised [75]) points towards the presence of numerous domains of random orientation. Indeed, such a hypothesis can be immediately proven by optical microscopy and was further confirmed by Michielsen *et al.* in 2010, who performed FDTD calculations to predict the scattering of light from gyroid domains with various orientations, the results of which agreed well with experimental data [52]. Similar macroscopic omnidirectionality of colour was also observed by other authors, with Saranathan *et al.* in 2010 additionally noting how photonic crystal domains with various orientations result in a broadening of the averaged reflectance peaks due to both single and multiple scattering of light from the different domains [14, 73]. It is interesting to note the strong biological significance of the observed colourations, e.g. camouflage, mate signalling and aposematic signalling to predators [14, 38, 76].

Finally, the polarisation-dependent optical response of gyroid photonic crystals was first confirmed experimentally in butterfly wing scales. Michielsen *et al.* in 2010 observed optical activity in gyroid biophotonic crystals [52]. In addition to optical activity, Mille *et al.* in 2011 and 2013 also observed circular dichroism in butterfly wing scales where some domains reflected light of one handedness with a greater intensity than light of the opposite handedness [51, 73]. However, it has also been demonstrated by Saba *et al.* in 2014 that the macroscopic reflections of *Callophrys rubi* and *Teinopalpus imerialis* exhibit no circular dichroism [20]. This is attributed primarily to a combination of structural effects, e.g. the polycrstallinity (and therefore multiple domain orientations) of the gyroid photonic crystals in the wing scale and the absorption due to a wavelength-selective pigment in the wing scales.

2.2.2. Biotemplated gyroids Although nature can provide various gyroid photonic crystals, their optical function is inherently limited by the low refractive index of the materials they are made from (e.g. 1.56 at 500 nm for chitin in butterfly wing scales [75]). As the photonic band gap of photonic crystals widens with increasing dielectric contrast (Table 1), various means to vary the dielectric contrast of biophotonic crystals through templating have been developed [77–83].

Mille *et al.* in 2011 successfully employed biotemplating to fabricate the first inorganic gyroid with a unit cell size comparable to the wavelength of visible light [73]. The authors employed a sol-gel method to replicate the internal structure of butterfly wing gyroid photonic crystals to create mesoporous silica inverse gyroids with a lower refractive index of 1.23 ± 0.05. As a result, the peak reflectivity of the silica gyroid blue-shifted to ~480 nm from the peak reflectivity of the chitin gyroid at ~540 nm.

Note that the ridges and cross-ribs which overlay the gyroid structure and modulate the spectral response of the wing scale (clearly visible in Fig. 10) [52] were not reproduced by this method.

The sol-gel methodology was subsequently improved by Mille *et al.* in 2013 by templating a gyroid butterfly wing scale into silica and titania [51]. The dielectric constant of the (inverse) gyroid structure was altered from that of chitin to 1.51 for silica and 4.28 for titania. Band structure calculations of the 65% fill fraction silica inverse gyroid predicted a decrease in (partial) band gap width, while the 50% fill fraction titania structure was predicted to increase, compared to the original chitin structure. Notwithstanding the shift in mid-gap frequency due to shrinkage of the replicated structures, the calculations accurately predict the variation in reflectivity spectra between the silica (maximum reflectivity $\sim$25%), chitin (maximum reflectivity $\sim$35%) and titania structures (maximum reflectivity $\sim$90%). Again, the ridges and cross-ribs of the butterfly wing scale were not replicated by this method, allowing the investigation of only the underlying gyroid structure.

Note that these examples of biotemplating do not achieve an exact replication of the gyroid structure, caused by unit cell shrinkage during processing (e.g. etching and annealing). The creation of a reliable template or mould for large area industrial processing remains a significant challenge. However, should such fabrication issues be overcome or otherwise mitigated, the potential for biotemplated photonic crystal replicas may be significant, with applications ranging from gas sensors to solar cells [69, 84–87].

2.2.3. "Top-down" gyroid assembly Despite advances in biotemplating, the direct synthesis of gyroid photonic crystals at various length scales from various organic and inorganic materials is desirable. Promising methods for 3D fabrication should be capable of mass-producing sub-µm periodic features over large areas and with a fine control of defects [40, 59]. To ensure a complete photonic band gap, all above conditions must also be realisable using high-dielectric constant materials. Ultimately, the preferred photonic material will offer the best compromise between the optical properties and ease of fabrication [49]. "Top-down" approaches currently offer one means of achieving gyroid photonic crystals with minimal defects operating in the near-infrared wavelength range.

Different top-down techniques are routinely used. Interference lithography is used to create three-dimensional structures, including the gyroid, through the superposition of coherent light in a photosensitive polymer [6, 88]. Alternatively, direct laser writing is used to create structures of arbitrary complexity in a photosensitive polymer by the translation of a focal spot in three dimensions [89–91]. This technique has recently been used with great success by Turner *et al.* to create gyroid photonic crystals operating in the microwave regime [44, 63]. Finally, 3D stereolithography (i.e. "3D printing") is used to create replicas of butterfly wing scale gyroid photonic crystals operating in the microwave regime [60].

Of recent interest has been the use of top-down fabrication techniques to tailor
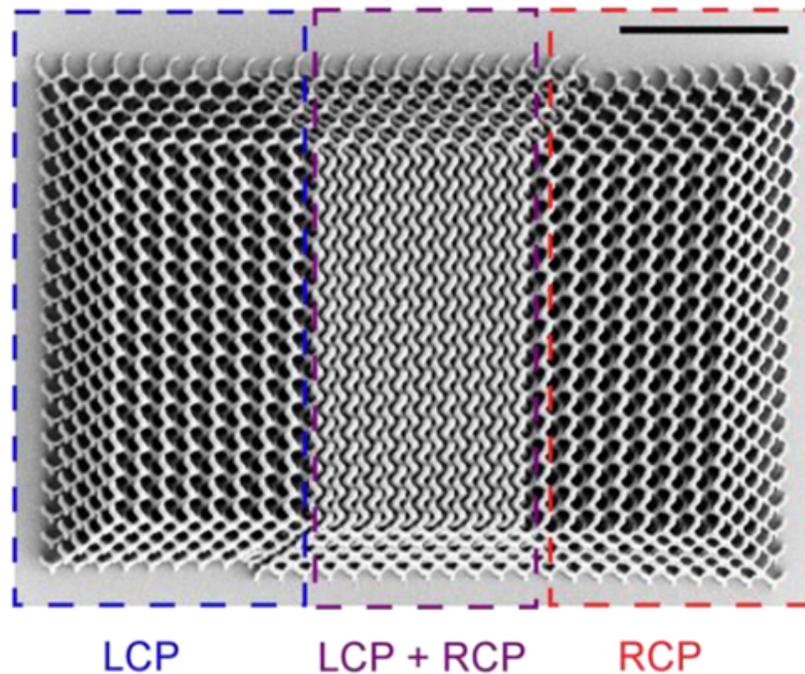
Figure 12. A top-down gyroid photonic crystal fabricated by direct laser writing; 15% fill fraction per single network, refractive index contrast of 1.48 and unit cell size 1.2 µm. The left most portion of the crystal has a handedness corresponding to left circularly polarised light (LCP), the right most portion a handedness corresponding to right circularly polarised light (RCP), and the mid-section an achiral composite of both left- and right-handed networks. Used with permission from [44].

the chiral properties of gyroid photonic crystals, including morphologies that are inaccessible in natural biophotonic gyroids (Fig. 12). In 2011, Turner *et al.* measured the transmission spectra for circularly polarised light of synthetic chiral composite photonic crystals based on interpenetrating gyroid networks [44]. The authors note that it is possible to arrange two, three, four and eight like-handed single gyroid networks into intertwining composites whilst maintaining an overall cubic structure and demonstrated the fabrication of an achiral and chiral composite from two opposite and similarly handed gyroid networks respectively [16]. Each polymer single gyroid network possessed a fill fraction of 15%, a unit cell size of 3 µm and a refractive index of 1.52, similar to the biological structures that inspired this study [13, 34, 38, 56, 75]. Whereas the achiral composite exhibited no circular dichroism (as evident from the transmission spectra) the chiral composite exhibited strong broadband circular dichroism and an associated circular dichroism stop band of around 6%, agreeing with the numerical predictions. The authors further investigated the effect of incident light on an interface between regions of different chirality (achiral and chiral of different handedness) and the circular polarisation conversion properties of the various chiral composites. The polarisation conversion was around 3.5% for a single or double gyroid network and between 20-50% for a chiral composite of two single gyroid networks of similar handedness.

More recently, in 2013, Turner *et al.* manufactured similar structures, fabricated by galvo-dithered direct laser writing, to realise a gyroid chiral beam splitter, a device challenging to produce given the lack of natural materials with circular birefringence [63]. The polymer chiral network, possessing a fill fraction of 30%, a unit cell size of 1.2 µm and a refractive index of 1.48, exhibited a strong circular dichroism at a wavelength of around 1.5 µm, often used in telecommunications, in good agreement with numerical predications (Fig. 13). By fabricating a triangular prism from the chiral network, the authors demonstrated the selective reflectance and transmission of incident circularly polarised light of different handedness. It was noted that the beam splitting was very much the result of the diffractive properties of the photonic crystal (the coupling of circularly polarised plane waves to Bloch modes of various polarisation states in the crystal) rather than a homogenous circular birefringence. Linear birefringence of the structure would lead to undesired circular polarisation conversion, which was avoided with the gyroid morphology.
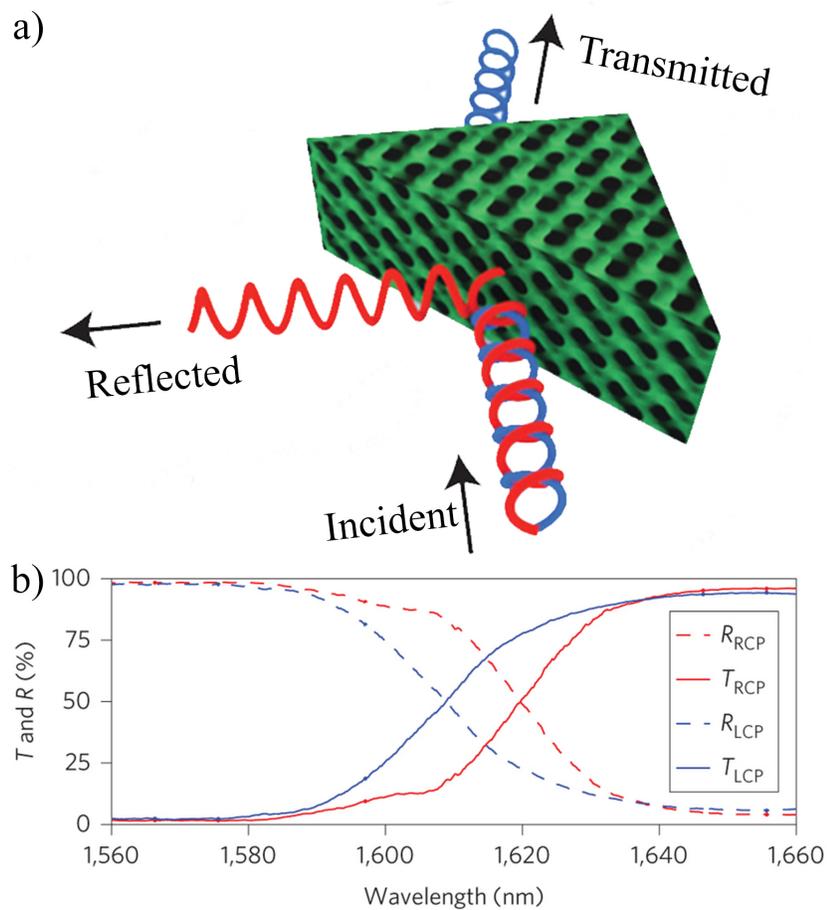
Figure 13. Reflection (dashed lines) and transmission (solid lines) spectra of right circularly polarised (RCP; red lines) and left circularly polarised (LCP; blue lines) light incident on a gyroid chiral beamsplitter, highlighting the circular dichroism of the structure. Reprinted by permission from Macmillan Publishers Ltd: Nature Photonics, copyright 2013

2.2.4. *"Bottom-up"* *gyroid* *assembly* Although top-down methods can create impressive gyroid photonic crystal structures not limited only to those found in nature, the "bottom-up" self-assembly of gyroid structures has been considered as a potential means to generate materials with a photonic band gap in the visible region of the spectrum. As already mentioned in Sect. 1.2, block copolymers are one such system in which the gyroid structure forms through self-assembly (see e.g. water-lipid phases [92]).

Unfortunately the periodicities of most block copolymer gyroids fall into the range 30-100 nm such that the mid-gap frequency of the photonic band gap resides in the ultraviolet region of the spectrum. Indeed, to the best knowledge of the authors, there has only been one example of gyroid self-assembly from block copolymers with a sufficiently large unit cell size to act as a photonic crystal close to the optical regime (the near ultraviolet). Urbas *et al.* in 2002 created a polystyrene-*block*-polyisoprene (PS-*b*-PI) double gyroid with a unit cell size of 258 nm (250 nm) as measured by x-ray scattering (electron microscopy) and a styrene filling fraction of 38% [37]. This double gyroid exhibited a reflectivity peak at 327 nm with a 70 nm width. To increase the dielectric contrast of the block copolymer gyroid (widening the photonic band gap) the low-ε phase of the structure was selectively etched to reduce its dielectric constant to that of air. As a result, the reflectivity peak shifted from 327 to 286 nm. Unfortunately, the authors do not discuss their results in terms of peak broadening, which is a benchmark for filling fraction change.

It is perhaps telling of the significant challenges associated with synthesising gyroid photonic crystals from block copolymers that there have been no published works improving upon the above results in over a decade. These challenges therefore remain and are explored below: the synthesis of appropriate triblock terpolymers which may be selectively etched to reveal a single gyroid structure; the increase in unit cell size of the self-assembled block copolymer gyroid; the increase in dielectric contrast of the structure; and the improvement of the long range order and orientation of the gyroid. The interested reader is directed towards a number of previous reviews which similarly explore these challenges in the context of one and two-dimensional block copolymer photonic crystals [61, 64].

Triblock terpolymer synthesis. Although a diblock copolymer may self-assemble into the double gyroid phase possessing two single gyroid networks, these networks are formed of the same block of the copolymer and are chemically indistinguishable. It is therefore impossible to selectively remove by any chemical means only one such network (perhaps along with the matrix phase) to leave either a single gyroid or single gyroid template. However, an equilibrium morphology formed by the self-assembly of a triblock terpolymer of appropriate composition may be similar to a double gyroid except that each of the two single gyroid networks and the matrix phase are chemically distinct, referred to as the "alternating gyroid" [93]. Triblock terpolymers synthesised such that one block may be selectively etched (e.g. by ozonolysis or dissolution) are therefore the material of choice for gyroid photonic crystals and further research is required to realise

such copolymers which also satisfy each of the further requirements presented below.

Large unit cell size. The unit cell sizes achievable in block copolymer gyroids are generally too small to produce a photonic band gap in the visible region of the spectrum. The approximate relationship is recalled whereby the mid-gap wavelength of a gyroid photonic crystal is roughly twice the lattice constant, which is proportional to the total degree of polymerisation N of the copolymer. Block copolymers which self-assemble into large unit cell gyroids must therefore have a large molecular weight. Unfortunately, such large molecular weight block copolymers are challenging to synthesise with the required low polydispersity. With the advent of polymer catalysis and radical polymerisation techniques, this synthesis is becoming easier (for a short summary of the modern synthesis of block copolymers and its recent advances see [94]). However, high molecular weight copolymers with exceptionally low polydispersities exhibit very slow self-assembly kinetics, prohibiting the self-assembly process which may yet prohibit the formation of the true equilibrium morphologies and good long range order over practical experimental time scales (as discussed in Sect. 1.2).

An alternative route to large unit cell gyroids is the swelling of the block copolymer domains with low molecular weight homopolymers. This has been attempted successfully for various block copolymer systems but a gyroid photonic crystal has yet to be demonstrated by this method [64, 95, 96]. However, this approach is complicated by the limitation that the homopolymer often phase separates from the copolymer. Only rather limited amounts of homopolymer may therefore be added, limiting the potential increase in unit cell size of the resulting gyroid. Instead, there may be greater scope in using a low molecular weight surfactants that associate with one block of the copolymer, e.g. by hydrogen bonding [97]. The resulting material retains a low viscosity at high temperatures due to the melting of the hydrogen bonds but "clicks" into place upon cooling. The strength of the intermolecular interactions between the surfactant and the associated block allows a high loading fraction of the surfactant, greatly increasing the resulting unit cell size of the gyroid.

Dielectric contrast. Generally, both the dielectric constant of each copolymer block and the dielectic contrast between the various blocks are small and therefore the resulting band gap (if existent) is likely to be incomplete and narrow. Block copolymer gyroid structures must be altered in order to maximise the dielectric contrast between the single gyroid network and the surrounding medium. One such method is to selectively remove unwanted phases, e.g. the matrix phase in the case of a double gyroid, as performed by Urbas *et al.* in 2002 [37]. Alternatively, the dielectric constant of the gyroid network could be increased by incorporating high-ε inorganic nanoparticles (e.g. cadmium selenide or gold) coated with an appropriate surfactant into one copolymer block [61, 64, 98, 99]. To the best of our knowledge there have been no attempts to infiltrate such high-ε nanoparticles into gyroid-forming block copolymers for photonic crystal applications.

However the perhaps most versatile means by which to increase the dielectric contrast of a block copolymer gyroid is to selectively etch one phase of the structure and back-fill the resulting "template" with an inorganic material of high dielectric constant, similar to biotemplating as discussed above [59,100–119]. In addition to a high refractive index, the chosen inorganic material should have high optical transmission (i.e. low loss; thus excluding metals) and high thermal and mechanical stability. Many options exist for the deposition of such a material including the choice between wet and dry fabrication processes and multiple or single templating steps (e.g. to recover either the etched phase or its inverse).

Dry deposition methods, such as chemical vapour deposition and atomic layer deposition, allow accurate control of the thickness of the deposited material. However, the main challenge of chemical vapour deposition into a porous template is the closure of pores before the template has been completely filled [59]. Such a "pinch-off" is undesirable as a reduced template fill fraction results in a lower band gap width for the structure. Although the pore sizes of triply periodic continuous structures are not generally uniform, such that pinch-off leaves behind unwanted interstitial voids, the gyroid morphology outperforms other similar structures in filling a greater fraction of the template before pinch-off. Moon *et al.* in 2007 predicted that it should be possible to achieve a 98% gyroid template fill fraction at pinch-off, with a corresponding band gap width of 98% of the theoretical maximum [100]. A lower template fill fraction and band gap width are expected experimentally, especially for nanoscale structures where the chemical vapour deposition process may additionally be limited by diffusion. Alternatively, wet chemical methods, including sol-gel reactions and electrodeposition, allow the complete deposition of various metals, metal chalcogenides and semiconductors. Indeed, a wet deposition method is much preferred to completely fill a porous template.

Long range order and orientation. The kinetic arguments presented to explain the inherent difficulties in achieving large unit cell gyroid block copolymers apply equally to the challenges of controlling long range order and orientation in such materials. The thermodynamic equilibrium morphology nucleates randomly and in multiple locations from a disordered copolymer melt, thereby resulting in numerous variously oriented microdomains. The kinetics of reorganisation of these microdomains during annealing (e.g. thermal or solvent vapour annealing) slows down with increasing viscosity of the melt and therefore the molecular weight of the copolymer. It is therefore a significant challenge to ensure that resulting structures exhibit the desired long range order and orientation as required by the majority of photonic or optical applications for which these materials are envisioned.

A number of strategies can be employed to increase the size of the microdomains or control their orientation. The microdomains can be enlarged either by suppressing the nucleation density of the equilibrium morphology (e.g. by quenching the melt very slowly during thermal annealing or using a very slow evaporation rate of solvent

during solvent vapour annealing) or annealing out the microdomain boundaries, thereby reorienting the domains (requiring usually long anneal times, but see [120]). Their orientation might also be affected by parameters such as the commensurability between the periodicity of the equilibrium morphology and the film thickness, the surface energies of the substrate-polymer and polymer-air interfaces, and the roughness of the substrate. Various techniques to direct the self-assembly of the copolymer have been attempted, e.g. the application of shear and electic fields or temperature gradients, and have been reviewed previously by Darling [24]. It should be noted that orientation control of the gyroid phase has typically been attempted via the orientation of another phase (e.g. hexagonally packed cylinders), from which the gyroid forms through an order-order transition upon removal of the field [33, 121, 122].

Two related and particularly promising techniques which have led to the demonstration of excellent long range order and orientational control for other block copolymer equilibrium morphologies (e.g. spheres or lamellae) are grapho- and chemoepitaxy. Both of these "directed self-assembly" methods seek to combine the accuracy and flexibility of standard top-down lithographic processes (e.g. electron beam lithography) with the small feature sizes achievable through bottom-up self-assembly. Graphoepitaxy is the topographic patterning of a substrate surface with features that are commensurate with the overlying copolymer film to induce order and orientation into the copolymer equilibrium morphology. For example, Bita *et al.* in 2008 used lithographically defined posts approximately 12 nm in diameter as a template for the spherical minority block of a polysytrene-*block*-polydimethylsiloxane (PS-*b*-PDMS) diblock copolymer [123]. The posts, fabricated from an electron beam resist, were functionalised with a homopolymer brush so that they chemically and physically resembled the minority block. Remarkable long range order was achieved even when the spatial frequency of the template was greater than that of the spheres. The patterned features need not necessarily be on the length scale of the block copolymer equilibrium morphology however, as evidenced in work by Segalman *et al.* in 2001 [124]. Instead, the hard or soft boundaries of relatively large channels and mesas were also observed to order block copolymer spheres. Chemoepitaxy is the chemical patterning of a substrate surface whereby the ordering and orientation is not induced by physical boundaries but rather by preferential thermodynamic interactions between patterned areas and the overlying block copolymer. For example, Kim *et al.* in 2003 demonstrated the epitaxial self-assembly and perfect registration of diblock copolymer lamellae onto a surface chemically patterned with a self-assembled monolayer [125]. However, it is generally the case that for the same degree of orientational control chemoepitaxy surfaces must be more densely patterned than graphoepitaxy surfaces.

Summary. Despite the challenges listed above, which have remained largely unresolved over the previous decade, the use of block copolymer self-assembly remains an extremely promising fabrication route to create gyroid photonic crystals operating in the visible regime. Many of the solutions which will be required to successfully fabricate the

desired single gyroid structure with a large unit cell size, large dielectric contrast, and large and controllably oriented microdomains arguably already exist. What remains is therefore to successfully combine these solutions, which does not seem to be an insurmountable challenge.

Until then, the current limitation on the achievable size of block copolymer gyroid unit cells may be used instead to great advantage in the creation of optical metamaterials, which by their very nature demand sub-wavelength feature sizes. It is this alternative use for existing gyroid block copolymers and the intriguing physics which they allow the exploration of which will be the focus of the remainder of this review. Of course, it must be noted that this alternative application of block copolymers sidesteps some but by no means all of the challenges listed above.

3. Gyroids on the sub-wavelength scale: metamaterials

Metamaterials are artificially engineered materials which, by virtue of their structure rather than their chemical composition, may exhibit various electromagnetic properties not otherwise encountered in nature (e.g. magnetism at optical frequencies). Unlike photonic crystals, the structural units of metamaterials, termed "meta-atoms" or "meta-molecules", are deeply sub-wavelength (e.g. by an order of magnitude). Therefore the response of the material can be described in terms of bulk (homogenous) effective parameters, i.e. permittivity ($\varepsilon_{\mathrm{eff}}$) or permeability ($\mu_{\mathrm{eff}}$). It is the nature and morphology of these structural units which imparts to a metamaterial its unique electromagnetic properties. One such property not generally found in nature but which has generated intense interest is negative refraction. Veselago in 1968 first theoretically demonstrated that a material with simultaneously negative values of ε and μ (a "doubly negative" medium) would exhibit negative refraction [126, 127]. However, without access to any natural doubly negative materials it was over thirty years until the phenomenon was first experimentally demonstrated, by Smith *et al.* in 2000, using split-ring resonator metamaterials [128]. That same year, Pendry made the first of a number of predictions regarding the potential applications of negatively refracting materials, namely that they could be used to create a lens capable of resolving sub-wavelength features [129]. Thus, the history of metamaterials since the turn of the century has been almost synonymous with the pursuit of negatively refracting materials.

Negative refraction is, however, only one electromagnetic property of potential interest. Indeed, the great attraction of metamaterials is that one may theoretically design any arbitrary electomagnetic response as desired (i.e. any $\varepsilon_{\mathrm{eff}}(\omega)$ and $\mu_{\mathrm{eff}}(\omega)$). Furthermore, some materials which would today be classified as metamaterials have in fact been studied for many decades (see e.g. [130] for a short history of the field). Those early metamaterials (e.g. artificial dielectrics [131]) were designed to operate in the microwave regime and were therefore macroscopic in their unit cell structure and periodicity. In contrast, an optical metamaterial requires structural units only tens of nanometres across in order to satisfy the condition of sub-wavelength feature sizes.

Achievements in the field of optical metamaterials have therefore gone hand in hand with advances in nanofabrication technologies, without which the ability to pattern materials on the required length scale would be near impossible (the interested reader is directed to an excellent review of metamaterial fabrication methods [132]).

An alternative route to negative refraction, other than the fabrication of a doubly negative medium, is to create a material with a strong chiral response [133]. If the chirality is sufficient, such a material will exhibit negative refraction for circularly polarised light [134,135]. It is for this reason, amongst others, that chiral metamaterials have also received intense interest (see [136] for a recent review of chiral metamaterials and [137] for a broader overview of chirality and chiro-optic effects in plasmonic structures).

A metallic gyroid fabricated using a block copolymer template inherently satisfies the requirement of an optical metamaterial (i.e. deeply sub-wavelength feature sizes) by virtue of the length scale of the self-assembly process. In addition, the structure is fully three-dimensional and intrinsically chiral, thus possibly also negatively refracting. Such three-dimensional (chiral) optical metamaterials simply cannot otherwise be fabricated over large areas with comparable rapidity using existing top-down fabrication techniques [132]. Gyroid metamaterials are therefore a rich source of interesting physics otherwise inaccessible by other means.

3.1. Experimental observations of gyroid optical metamaterials

Unlike gyroid photonic crystals which were studied first theoretically before their experimental demonstration, it was the intriguing results of early experiments which motivated the detailed theoretical investigation of metamaterial gyroids and their operation. The observed optical properties of gyroid metamaterials are therefore presented first, along with a simple and intuitive model by which to understand their spectral response, before the more detailed current theoretical understanding of their electromagnetic behaviour is described.

Gyroid metamaterials working at optical frequencies were first fabricated and demonstrated by Vignolini *et al.* in 2012 [138]. Working with a polyisoprene-*block*-polystyrene-*block*-polyethylene oxide (PI*b*-PS-*b*-PEO or simply ISO) triblock terpolymer, the authors selectively removed the polyisoprene phase from the self-assembled gyroid structure by ozonolysis to leave behind a single gyroid template. This template was then back-filled with gold by electrodeposition to create, upon removal of the remaining organic material, a gold single gyroid thin film of roughly 200 nm in thickness (Fig. 14). The gold gyroid structure possessed a unit cell size of around 50 nm and a fill fraction of 30% [138, 139]. Note that gold was chosen because of its plasmonic properties and chemical stability. Reflection and transmission spectra of the gold gyroid thin film were obtained using unpolarised light, highlighting the characteristic gyroid extinction peak at around 600 nm. Investigation of individual domains (between 10-100 μm in size) allowed identification of both linear and circular

dichroism in the samples (Fig. 15). Circular dichroism was not observed along the [110] direction but instead occurred when the incident light coincided with the [111] chiral axis of the gyroid structure (see Fig. 2).
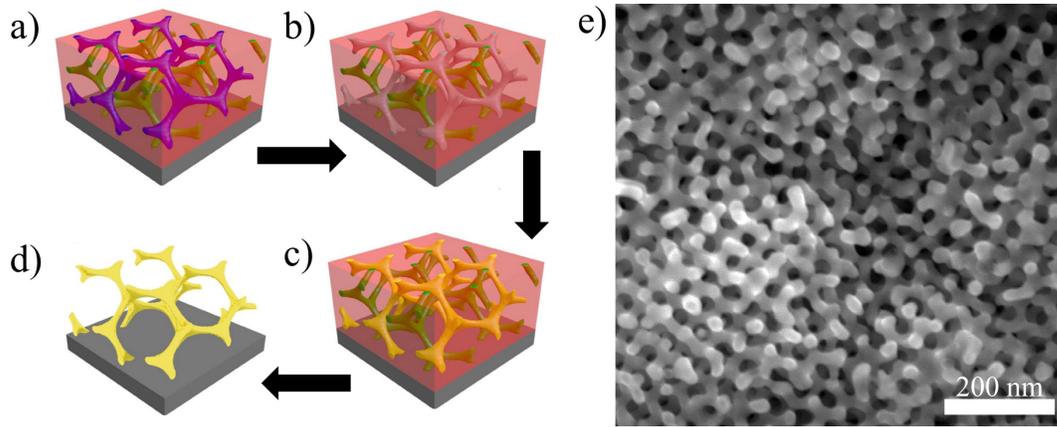
Figure 14. Fabrication process of gyroid metamaterials from block copolymers. a) Gyroid equilibrium morphology formed from a triblock terpolymer (red, blue and green). b) Selective etching of a single gyroid network (i.e. one copolymer block; blue) resulting in a single gyroid template. c) Back-filling of the gyroid template with metal (e.g. gold; yellow) by electrodeposition. d) Removal of the remaining organic material (red and green) resulting in a gyroid metamaterial. e) Scanning electron micrograph of a 50 nm unit cell gold gyroid with a fill fraction of around 30%.

The spectral response of the gold gyroid metamaterial described above was first explained intuitively with respect to the classic sparse cubic wire array investigated by Pendry *et al.* in 1996, which exhibits a greatly reduced plasma frequency [3]. As part of their study, Vignolini *et al.* noted that an amorphous composite of gold and air at the same fill fraction should exhibit near-perfect reflection in the red and infrared, contrary to the experimental results [138]. It was therefore hypothesised that the gyroid metamaterial acted as a metal with an effective plasma frequency substantially reduced from that of gold (from 7.5 eV to 1.55 eV when modelled as a Drude metal). According to the model, such a decrease in plasma frequency comes about from both a reduction in average electron density due to the porosity of structure and the increased self-inductance of the highly interconnected and ordered network of metal. It was with respect to this simple model that many of the initial experimental results were explained.

Salvatore *et al.* further investigated the potential to tune the optical properties of similar gold gyroid metamaterials by three distinct mechanisms: the unit cell size; the fill fraction; and the refractive index of the surrounding media [140]. Using two ISO triblock terpolymers of different molecular weights but identical block volume fractions (and therefore fill fractions), the authors first demonstrated the shift in extinction peak caused by variation in unit cell size. The two terpolymers formed gyroids with 35 and 50 nm unit cell sizes and exhibited extinction peaks at 550 and 620 nm respectively. The fill fraction of either gyroid could be increased by electrodepositing additional metal onto gold gyroid material from 30% up to 90%. As the fill fraction increased, the
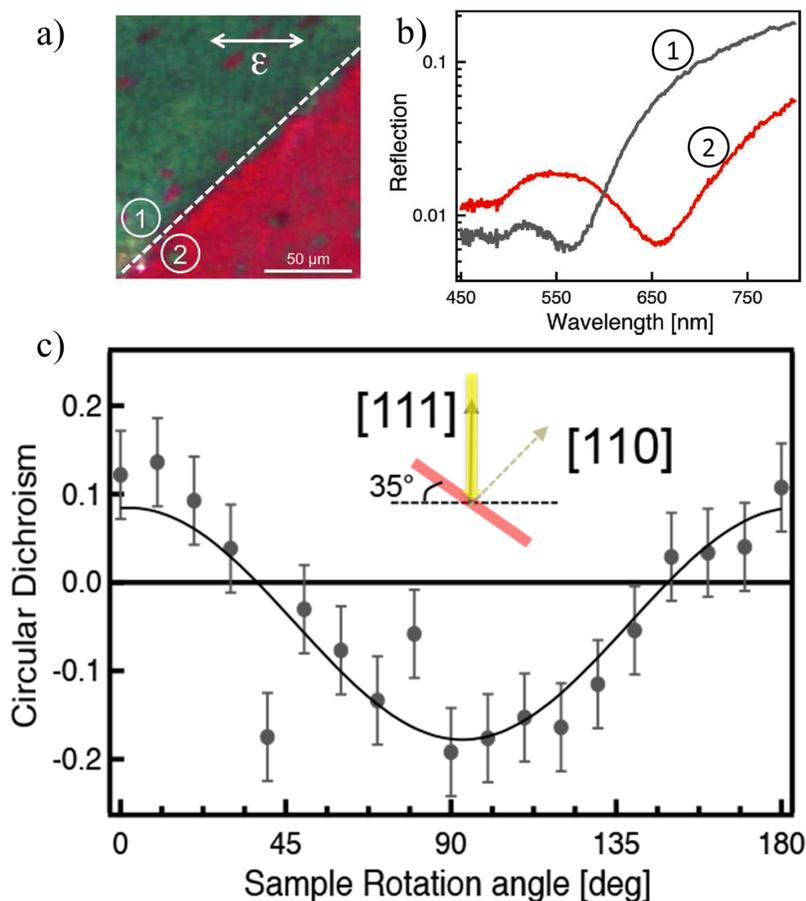
Figure 15. Linear and circular dichroism of gold gyroid metamaterials. a) Optical micrograph of a 50 nm unit cell and 30% fill fraction gold gyroid metamaterial under linearly polarised light (as indicated by the white arrow); regions labelled "1" and "2" are two domains for which the orientation of the gyroid is roughly parallel to and perpendicular to the [100] axis respectively. b) Reflection spectra of the two domains visible in the optical micrograph. c) Difference between the transmission (averaged over the wavelengths 600 to 750 nm) for right- and left-handed circularly polarised light for the same gyroid when rotated around the [110] axis at an angle of 35° to the horizontal. The solid line is a guide for the eye, see [138].

extinction peak and the "plasma edge" (qualitatively similar to the plasma wavelength) both blue-shifted due to the modification of the mobility of electrons in the larger struts. Also noticeable with the increase in fill fraction was the reduction in linear dichroism of the structure. The linear dichroism reduced from its maximum at a fill fraction of 30% to zero for fill fractions greater than 50%. Finally, the extinction peak was further varied by infiltration of the structure with media of various refractive indices, thereby changing the dielectric contrast. As the refractive index of the surrounding medium was successively increased from that of air to that of an oil with refractive index of 1.7, the extinction peak and plasma edge red-shifted by around 200 nm.

3.2. Theoretical predictions of gyroid optical metamaterials

Although the intuitive model introduced above describes well some aspects of the gyroid metamaterial electromagnetic response, it fails to model its inherent chirality and associated polarisation dependent response. Chirality is of significant interest in the field of metamaterials as it offers the possibility of negative refraction and opportunities to manipulate various polarisation effects (e.g. circular dichroism and optical activity [137]). Developed by Demetriadou *et al.* in 2013 and further elucidated by Oh *et al.* the same year, the tri-helical metamaterial (THM) model was proposed as an analytical model to investigate the (chiral) electromagnetic response of gyroid metamaterials and their underlying physics [141, 142]. The THM model approximates the single gyroid structure as a network of unconnected helices oriented along the three cubic axes (Fig. 16a). The model allows the identification of two transverse and one longitudinal propagating mode and their dispersion relations, which were found to agree well with FDTD band calculations of a perfect electrical conductor (PEC) THM. As expected, due to the strong chirality of the structure, the two transverse modes were non-degenerate, leading to negative refraction for one circular polarisation. However, an FDTD band calculation of a PEC gyroid along the [100] and [111] directions highlighted no such degeneracy of the transverse modes for k values away from the Brillouin zone boundaries, implying that the gyroid possesses significantly weaker chirality than the THM. Further investigation of the magnetic fields associated with the propagating longitudinal and transverse modes in the gyroid determined that they are highly localised along the smaller helices present in the structure (Fig. 16b and c). These smaller helices therefore dominate and determine the electromagnetic response of the metamaterial. It is this dominance, the interconnectivity of the structure, and the mixture of right- and left-handed helices present along any orientation of the gyroid which appear to be responsible for the significant weakening of its chirality and the absence of negative refraction [141, 142].

Although it incorrectly predicts negative refraction, the THM model may still be applied to the PEC gyroid, using the geometrical parameters of the small helices, to predict with reasonable accuracy the plasma frequency of the metamaterial. Confirming the qualitative explanation offered previously, the plasma frequency is indeed significantly red-shifted due to the self-inductance of the structure. Notwithstanding the effect of a finite cross-coupling between circular polarisations upon the reflection and transmission spectra for light incident on a finite slab of PEC gyroid, the spectra also differ significantly for right- and left-handed circularly polarised light, confirming theoretically the circular dichroism of the metamaterial particularly along the [111] and [100] directions [142].

Whereas the comparison between the PEC THM and gyroid allows the identification of structural contributions to the electromagnetic response of the gyroid metamaterial, the comparison between a PEC and gold gyroid highlights the material contribution. A gyroid composed of gold (modelled as a Drude metal) was calculated
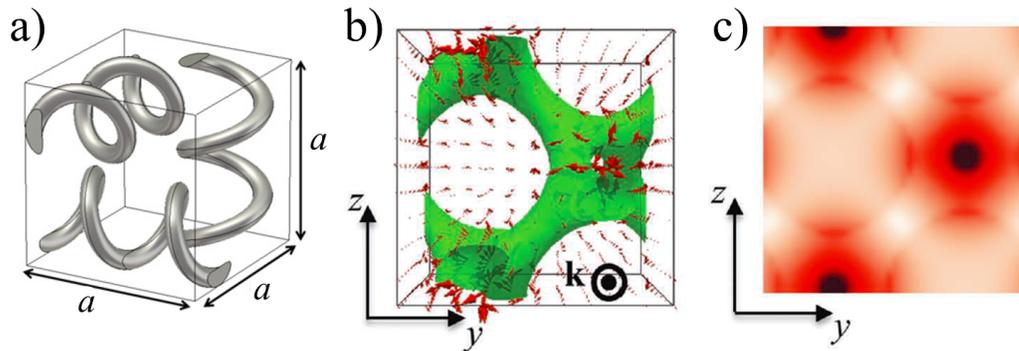
Figure 16. a) Tri-helical metamaterial approximation of the gyroid, where a is the unit cell size. Used with permission [141]. b) Magnetic field distribution within a PEC gyroid demonstrating the dominance of the small helices on the optical properties. Magnetic field vectors (arrows) at a point in time during propagation of the longitudinal mode travelling in the x-direction (into the page). c) The line-integral along the x-direction of the square of the magnetic field strength; dark and light represent areas of maxima and minima of the field strength respectively. Used with permission [142].
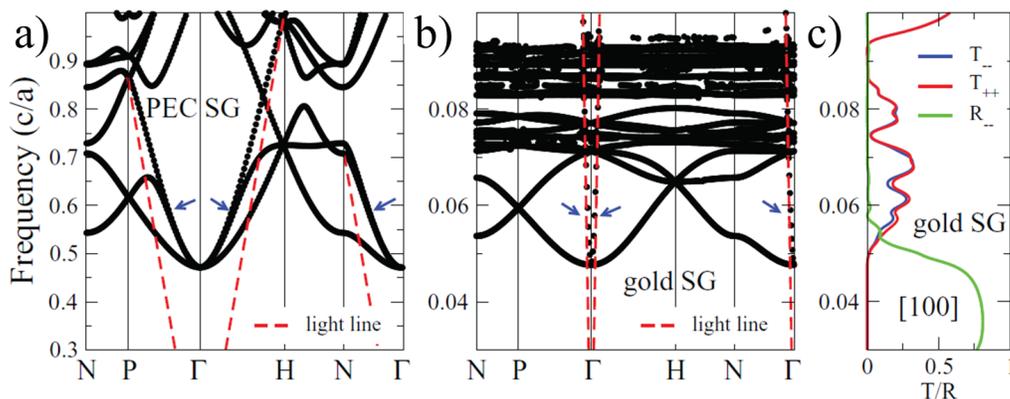
Figure 17. Gyroid metamaterial band diagrams and transmission and reflection spectra. a) Band diagram for a PEC gyroid with 40 nm unit cell size and 10% fill fraction. b) Band diagram of an equivalent gold gyroid modelled as a Drude metal. c) Transmission and reflection spectra of the same gold gyroid along the [100] direction. The subscripts "++" and "−−" refer to right and left circularly polarised light respectively. Used with permission [142].

to exhibit bands which were red-shifted ten-fold compared to the PEC gyroid due to the penetration of the electromagnetic field into the wires (Fig. 17). Accounting for the induced current resulting from complete penetration of the metal by the surrounding electromagnetic fields allows the analytical derivation of the plasma frequency of a gold THM. Using this improved THM model allows quantitative prediction of the effect of unit cell size, fill fraction, and host dielectric constant on the optical properties of the metamaterial. Differences between the analytical and numerically calculated plasma wavelength were attributed to high density localised plasmon modes not accounted for

in the model. These localised plasmon modes, resulting from the three-dimensional structure of the gyroid, appear relatively fixed in frequency as the fill fraction of the gyroid increases, unlike the propagating modes. When the fill fraction is around 30%, that of the experimentally fabricated gold gyroids [138], the propagating modes are immersed in the frequency range of the localised plasmon modes which, due to their absorbtive character, affect the numerical transmission and reflection spectra. Again, circular dichroism is identified in the gold gyroid, but the dichroism is much smaller than for the PEC gyroid. This is attributed to improved impedance matching between the gyroid and its surroundings, the penetration of the electromagnetic field into the gyroid, and increased losses. Material properties therefore appear to affect the circular dichroism of the metamaterial gyroid more significantly than its structural properties.

Recently a more elegant set of approximate analytical expressions for the permittivity and extinction peak of the gold gyroid metamaterial have been derived [143]. Building on the above THM work, Farah *et al.* demonstrate that the effective permittivity of the gold gyroid $\varepsilon_{\mathrm{gyr}}$ can be approximated as

$$\varepsilon_{\mathrm{gyr}} = \frac{l\sqrt{2}}{a}\left[1 - \left(\frac{4r_{\mathrm{g}}}{\lambda_{\mathrm{g}}}\right)^2\left(\frac{\pi\sqrt{-\varepsilon_{\mathrm{m}}}}{2\sqrt{2}n_{\mathrm{fill}}} - 1\right)^2\right], \qquad (5)$$

where l is the normalised helix length, a is the unit cell size, $r_{\mathrm{g}} \approx 0.29a\sqrt{f}$ is the thinnest radius of the gyroid strut, f is the fill fraction, n_{fill} is the refractive index of the surrounding medium and λ_{g} is the effective plasma wavelength of a PEC gyroid. Finally, ε_{m} is the permittivity of gold when fashioned into 10 nm diameter struts, e.g. taking into account the polycrystalline nature of the metal. Furthermore, the wavelength of the extinction peak was also derived based on a number of further simple assumptions given the condition that minimum reflection occurs when $\varepsilon_{\mathrm{gyr}} = \varepsilon_{\mathrm{air}} = 1$ (or alternatively $\mathrm{Re}\left\{\varepsilon_{gry}\right\} = 1$). The wavelength of the dip in reflectivity λ_{dip} is therefore given as

$$\frac{\lambda_{\mathrm{dip}}^2}{\lambda_{\mathrm{p}}^2} = \varepsilon_{\infty} + \frac{8n_{\mathrm{fill}}^2}{\pi^2}\left(1 + \frac{\eta\lambda_{\mathrm{g}}}{4r_{\mathrm{g}}}\right)^2, \qquad (6)$$

where, e.g. for gold modelled as a Drude metal, $\lambda_{\mathrm{p}} = 146\,\mathrm{nm}$, $\varepsilon_{\infty} = 7$ and $\eta^2 = 1 - a/l\sqrt{2}$. Despite the inability of the model to account for the differing optical response of the gyroid for different polarisation states and orientations, the above equation was shown to predict remarkably well the extinction peaks in the reflection spectra for a 35 nm gold gyroid with different refractive indices of the surrounding medium.

Whereas all experimental studies have thus far been performed on single gyroids, the research to first highlight the potential for metallic gyroids to act as metamaterials, by Hur *et al.* in 2011, investigated also double and "hollow" double gyroids [144]. The authors notably predicted negative refraction for low-loss (e.g. silver or aluminium) double gyroids in the visible and near-infrared. Lossless gold double gyroids with a 100 nm unit cell size and a 34% fill fraction did not exhibit a metallic band gap but instead showed low frequency bands, not otherwise expected considering the high volume fraction of metal. Closer investigation of these low frequency propagation

Table 2. Effect of increase in various structural parameters on the effective plasma wavelength λ_p and linear and circular dichroism of gyroid metamaterials. ↑ indicates a proportional relationship, ↓ an inverse relationship, and "–" that the relationship is as yet unexplored.

	λ_p	Linear and circular dichroism
Unit cell size (a)	↑	↓
Fill fraction (ϕ)	↓	↓
Dielectric matrix (ε)	↑	–

bands revealed that some exhibited all-angle negative refraction. The introduction of damping losses had little effect on the negative refraction band. However, utilisation of an experimentally derived dielectric constant for gold highlighted the prevention of negative refraction by the strong absorption resulting from interband transitions [144]. It was hypothesised that the two single gyroid networks which comprise the double gyroid form a capacitor structure via the coupled surface plasmon resonances of the two individual networks. This capacitor may act as a metal-insulator-metal waveguide, which supports surface plasmon polariton propagation, and the resulting waveguide bands were found to be responsible for the negative refraction. Note that according to this hypothesis the negative refraction predicted in double gyroids is clearly not a product of the chirality of the structure, which is overall achiral. Though given less attention, single gyroids (termed "alternating" gyroids) were also investigated. Lacking a "counter electrode", the low frequency propagation of light from coupled surface plasmon resonances was forbidden and single gyroids therefore demonstrated a metallic band gap at low frequencies. Note that no experimental evidence has yet been offered of negative refraction in metallic double gyroids.

In summary, gold gyroid metamaterials fabricated via block copolymer self-assembly support localised and propagating low frequency plasmon modes with a greatly reduced plasma frequency from that of bulk gold. Their optical properties vary with unit cell size, fill fraction and the dielectric of the surrounding medium. Additionally, these metamaterials exhibit both linear and circular dichroism. The effect of the various structural and material parameters on the response of the gyroid metamaterial as explored above are summarised in Table 2.

4. Conclusion and outlook

This review explores the optical properties of gyroid structured materials structured on two distinct length scales. Where the material has been patterned on a length scale similar to the wavelength of light, the optical properties of the resulting gyroid photonic crystal are determined by the constructive light interference from the multiple refractive index boundaries present in the structure. Such gyroid photonic crystals are

predicted to exhibit a photonic band gap which is complete given a sufficiently large dielectric contrast and an appropriate choice of fill fraction of the high-ε phase. These photonic crystals are also predicted to exhibit both linear and circular dichroism and optical activity. Examples of gyroid photonic crystals may be found in nature, such as in the wing scales of some butterflies species, allowing experimental confirmation of the predicted optical properties. However, synthetic gyroid photonic crystals, fabricated either bottom-up using block copolymers or top-down using laser writing techniques, have yet to demonstrate successful operation in the visible region of the spectrum. Instead, the use of block copolymers allows the creation of gyroid metamaterials, for which the unit cell size is significantly smaller than the wavelength of light. These gyroid metamaterials exhibit optical properties determined by the sub-wavelength structure and electronic interactions of the constituent material (e.g. gold). These properties again include linear and circular dichroism and optical activity, although the interconnectivity and mixed chirality of the single gyroid may preclude negative refraction. Instead, it is the double gyroid which is predicted to exhibit negative refraction, though yet to be demonstrated experimentally.

The similarities between natural and artificial self-assembled systems are intriguing. For example, both in biological gyroids in butterfly wing scales and in gyroids self-assembled from block copolymers the [110] orientation has been observed to orientate preferentially out of plane [74, 138]. This highlights the strong role of the substrate surface which might potentially affect the self-assembly process *in vitro* in block copolymers and *in vivo* in butterfly wing scales. It will be interesting to further investigate these aspects.

The unique geometrical properties of the gyroid and its startling occurrence in self-assembled natural and synthetic systems continue to assure that the morphology is of significant interest both as a photonic crystal and as a metamaterial. In both instances the chiral properties of the structure and the resulting optical activity and circular dichroism have attracted most interest. With regards to synthetic gyroid photonic crystals, there is a pressing need to fabricate structures of appropriate unit cell size such that the photonic band gap resides within the visible region of the spectrum. This should ideally be achieved whilst also using high dielectric constant materials and with significant long range order. Block copolymers are one potential means by which to fulfil these requirements, but the experimental realisation remains challenging. A large molecular weight triblock terpolymer with high etch selectivity and large dielectric contrast has been an explicit goal for at least a decade but one which, as yet, has remained elusive. Whether the aim is photonic crystals or metamaterials, the judicious combination of top-down lithographic and bottom-up self-assembly methods (e.g. grapho- or chemoepitaxy) will almost certainly be required to ensure both long range order and orientational control of the structure. However, the natural length scales of small to medium molecular weight block copolymers already available are ideal for the templated fabrication of optical metamaterials. Indeed, gyroid metamaterials from block copolymers represent one of the very few self-assembled three-dimensional

(chiral) optical metamaterials in existence.

Acknowledgments

References

[1] E. Hecht. *Optics*. Addison Wesley Publishing Company, **1997**.

[2] F. Capolino. *Applications of Metamaterials*. CRC Press, **2009**.

[3] J. Pendry, A. Holden, W. Stewart, and I. Youngs. *Phys Rev Lett* **1996**, *76*, 4773.

[4] R. A. Shelby, D. R. Smith, and S. Schultz. *Science* **2001**, *292*, 77.

[5] J. Fleming, S. Lin, I. El-Kady, R. Biswas, and K. Ho. *Nature* **2002**, *417*, 1548.

[6] M. Maldovan and E. L. Thomas. *Nat Mater* **2004**, *3*, 593.

[7] P. Vukusic and J. R. Sambles. *Nature* **2003**, *424*, 852.

[8] J. D. Joannopoulos, S. G. Johnson, J. N. Winn, and R. D. Meade. *Photonic Crystals: Molding the Flow of Light (Second Edition)*. Princeton University Press, **2008**.

[9] A. H. Schoen. 'Infinite periodic minimal surfaces without self-intersections.' Technical Notes TN D-5541, NASA, **1970**.

[10] A. H. Schoen. *Interface Focus* **2012**, *2*, 658.

[11] S. Hyde. *The Language Of Shape: The Role Of Curvature In Condensed Matter: Physics, Chemistry and Biology*. Elsevier, Amsterdam,, **1997**.

[12] M. Wohlgemuth, N. Yufa, J. Hoffman, and E. L. Thomas. *Macromolecules* **2001**, *34*, 6083.

[13] K. Michielsen and D. G. Stavenga. *J Roy Soc Interface* **2008**, *5*, 85.

[14] V. Saranathan, C. O. Osuji, S. G. J. Mochrie, H. Noh, and S. Narayanan. *Proc Natl Acad Sci USA* **2010**, *107*, 11676.

[15] G. E. Schröder-Turk, S. Wickham, H. Averdunk, F. Brink, J. D. Fitz Gerald, L. Poladian, M. C. J. Large, and S. T. Hyde. *J Struct Biol* **2011**, *174*, 290.

[16] M. Saba, M. Thiel, M. Turner, and S. Hyde. *Phys Rev Lett* **2011**, *103902*, 1.

[17] L. Lu, L. Fu, J. D. Joannopoulos, and M. Soljac. *Nat Photonics* **2013**, *7*, 294.

[18] M. Saba, M. D. Turner, K. Mecke, M. Gu, and G. E. Schr. *Phys Rev B* **2013**, *88*, 245116.

[19] K. Grosse-Brauckmann. *J Colloid Interf Sci* **1997**, *187*, 418.

[20] M. Saba, B. D. Wilts, J. Hielscher, and G. Schroder-Turk. *Mater Today Proc* **2014**, page in press.

[21] S. T. Hyde and G. E. Schrder-Turk. *Interface Focus* **2012**, *2*, 529.

[22] J. N. L. Albert, T. D. Bogart, R. L. Lewis, K. L. Beers, M. J. Fasolka, J. B. Hutchison, B. D. Vogt, and T. H. Epps. *Nano Lett* **2011**, *11*, 1351.

[23] R. a. Segalman. *Materials Science and Engineering: R: Reports* **2005**, *48*, 191.

[24] S. Darling. *Prog Polym Sci* **2007**, *32*, 1152.

[25] K. Koo, H. Ahn, S.-W. Kim, D. Y. Ryu, and T. P. Russell. *Soft Matter* **2013**, *9*, 9059.

[26] M.-S. She, T.-Y. Lo, H.-Y. Hsueh, and R.-M. Ho. *NPG Asia Materials* **2013**, *5*, e42.

[27] Y. Mai and A. Eisenberg. *Chem Soc Rev* **2012**, *41*, 5969.

[28] I. Hamley. *Prog Polym Sci* **2009**, *34*, 1161.

[29] J. Cheng, C. Ross, H. Smith, and E. Thomas. *Adv Mater* **2006**, *18*, 2505.

[30] M. R. J. Scherer. *Double-Gyroid-Structured Function Materials.* Springer, 2013 editi ed., **2013**.

[31] E. W. Cochran, C. J. Garcia-Cervera, and G. H. Fredrickson. *Macromolecules* **2006**, *39*, 2449.

[32] M. E. Vigild, K. Almdal, K. Mortensen, J. P. A. Fairclough, and A. J. Ryan. *Macromolecules* **1998**, *31*, 5702.

[33] C.-Y. Wang and T. P. Lodge. *Macromolecules* **2002**, *35*, 6997.

[34] S. Kinoshita. *Structural Colors in the Realm of Nature.* World Scientific Publishing Company, Singapore, **2008**.

[35] S. John. *Phys Rev Lett* **1987**, *58*, 2486.

[36] E. Yablonovitch. *Phys Rev Lett* **1987**, *58*, 2059.

[37] B. A. M. Urbas, M. Maldovan, P. Derege, and E. L. Thomas. *Adv Mater* **2002**, *14*, 1850.

[38] B. D. Wilts, K. Michielsen, H. De Raedt, and D. G. Stavenga. *Interface Focus* **2011**, *2*, 681.

[39] P. Braun, S. Rinne, and F. Garca-Santamara. *Adv Mater* **2006**, *18*, 2665.

[40] K. Ishizaki, M. Koumura, K. Suzuki, K. Gondaira, and S. Noda. *Nat Photon* **2013**, *7*, 133.

[41] V. R. Almeida, C. A. Barrios, R. R. Panepucci, and M. Lipson. *Nature* **2004**, *431*, 1081.

[42] G. A. Ozin and S. M. Yang. *Adv Funct Mater* **2001**, *11*, 95.

[43] A. Chutinan, S. John, and O. Toader. *Phys Rev Lett* **2003**, *90*, 123901.

[44] M. D. Turner, G. E. Schröder-Turk, and M. Gu. *Opt Express* **2011**, *19*, 10001.

[45] L. Martin-Moreno, F. J. Garcia-Vidal, and A. M. Somoza. *Phys Rev Lett* **1999**, *83*, 73.

[46] V. Babin, P. Garstecki, and R. Hoyst. *Phys Rev B* **2002**, *66*, 235120.

[47] M. Maldovan, A. Urbas, N. Yufa, W. Carter, and E. Thomas. *Phys Rev B* **2002**, *65*, 165123.

[48] K. Michielsen and J. Kole. *Phys Rev B* **2003**, *68*, 115107.

[49] M. Maldovan, W. C. Carter, and E. L. Thomas. *Appl Phys Lett* **2003**, *83*, 5172.

[50] B. D. Wilts, K. Michielsen, H. De Raedt, and D. G. Stavenga. *J Roy Soc Interface* **2012**, *9*, 1609.

[51] C. Mille, E. C. Tyrode, and R. W. Corkery. *RSC Advances* **2013**, *3*, 3109.

[52] K. Michielsen, H. De Raedt, and D. G. Stavenga. *J Roy Soc Interface* **2010**, *7*, 765.

[53] B. D. Wilts, K. Michielsen, H. De Raedt, and D. G. Stavenga. *Proc Natl Acad Sci USA* **2014**, *111*, 4363.

[54] A. Taflove, S. G. Johnson, and A. Oskooi. *Advances in FDTD Computational Electrodynamics: Photonics and Nanotechnology.* Artech House, **2013**.

[55] A. Taflove and S. C. Hagness. *Computational Electrodynamics: The Finite-Difference Time-Domain Method.* Artech House, **2000**.

[56] L. Poladian, S. Wickham, K. Lee, and M. C. J. Large. *J Roy Soc Interface* **2009**, *6 Suppl 2*, S233.

[57] M. M. Sigalas, C. M. Soukoulis, C. T. Chan, R. Biswas, and K. M. Ho. *Phys Rev B* **1999**, *59*, 12767.

[58] Z.-Y. Li and Z.-Q. Zhang. *Phys Rev B* **2000**, *62*, 1516.

[59] J. H. Moon and S. Yang. *Chem Rev* **2010**, *110*, 547.

[60] C. Pouya and P. Vukusic. *Interface Focus* **2012**, *2*, 645.

[61] B. A. C. Edrington, A. M. Urbas, P. Derege, C. X. Chen, T. M. Swager, N. Hadjichristidis, M. Xenidou, L. J. Fetters, J. D. Joannopoulos, Y. Fink, and E. L. Thomas. *Adv Mater* **2001**, *13*, 421.

[62] C. T. Chan, K. M. Ho, and C. M. Soukoulis. *EPL* **1991**, *16*, 563.

[63] M. D. Turner, M. Saba, Q. Zhang, B. P. Cumming, G. E. Schröder-Turk, and M. Gu. *Nat Photonics* **2013**, *7*, 801.

[64] J. Yoon, W. Lee, and E. L. Thomas. *MRS Bull* **2005**, *30*, 721.

[65] H.-Y. Hsueh, Y.-C. Ling, H.-F. Wang, L.-Y. C. Chien, Y.-C. Hung, E. L. Thomas, and R.-M. Ho. *Adv Mater* **2014**, *26*, 3225.

[66] J. J. K. Kirkensgaard, M. E. Evans, L. de Campo, and S. T. Hyde. *Proc Natl Acad Sci USA* **2014**, *111*, 1271.

[67] M. Turner, G. Schroder-Turk, and M. Gu. In 'Laser Technology in Biomimetics,' (Eds. V. Schmidt and M. R. Belegratis), Springer, Berlin, pages 67–82. **2013**, .

[68] G. E. Schröder-Turk, A. Fogden, and S. T. Hyde. *Eur Phys J B* **2006**, *54*, 509.

[69] R. A. Potyrailo, H. Ghiradella, A. Vertiatchikh, K. Dovidenko, J. R. Cournoyer, and E. Olson. *Nat Photonics* **2007**, *1*, 123.

[70] J. W. Galusha, L. R. Richey, J. S. Gardner, J. N. Cha, and M. H. Bartl. *Phys Rev E* **2008**, *77*, 050904.

[71] A. R. Parker and H. E. Townley. *Nat Nanotechnol* **2007**, *2*, 347.

[72] A. R. Parker. *J Opt A* **2000**, *2*, R15.

[73] C. Mille, E. C. Tyrode, and R. W. Corkery. *Chem Commun* **2011**, *47*, 9873.

[74] S. Yoshioka, H. Fujita, S. Kinoshita, and B. Matsuhana. *J Roy Soc Interface* **2014**, *11*, 20131029.

[75] H. L. Leertouwer, B. D. Wilts, and D. G. Stavenga. *Opt Express* **2011**, *19*, 24061.

[76] S. M. Doucet and M. G. Meadows. *J Roy Soc Interface* **2009**, *6 Suppl 2*, S115.

[77] M. R. Jorgensen and M. H. Bartl. *J Mater Chem* **2011**, *21*, 10583.

[78] J. Huang, X. Wang, and Z. L. Wang. *Nano Lett* **2006**, *6*, 2325.

[79] Y. Tan, J. Gu, X. Zang, W. Xu, K. Shi, L. Xu, and D. Zhang. *Angew Chem Int Ed* **2011**, *123*, 8457.

[80] M. Lai, A. N. Kulak, D. Law, Z. Zhang, F. C. Meldrum, and D. J. Riley. *Chem Commun* **2007**, *1*, 3547.

[81] J. W. Galusha, L. R. Richey, M. R. Jorgensen, J. S. Gardner, and M. H. Bartl. *J Mater Chem* **2010**, *20*, 1277.

[82] J. W. Galusha, M. R. Jorgensen, and M. H. Bartl. *Adv Mater* **2010**, *22*, 107.

[83] D. Van Opdenbosch, M. Johannes, X. Wu, H. Fabritius, and C. Zollfrank. *Phot Nanostruct* **2012**, *10*, 516.

[84] L. Biró, K. Kertész, Z. Vértesy, and Z. Bálint. In 'Optical Engineering+ Applications,' International Society for Optics and Photonics, **2008**, pages 705706–705706.

[85] L. P. Biro and J.-P. Vigneron. *Laser Photon Rev* **2011**, *5*, 27.

[86] S. Guldin, S. Huttner, M. Kolle, M. E. Welland, P. Muller-Buschbaum, R. H. Friend, U. Steiner, and N. Tetreault. *Nano Lett* **2010**, *10*, 2303.

[87] D.-H. Ko, J. R. Tumbleston, L. Zhang, S. Williams, J. M. DeSimone, R. Lopez, and E. T. Samulski. *Nano Lett* **2009**, *9*, 2742.

[88] C. K. Ullal, M. Maldovan, E. L. Thomas, G. Chen, Y.-J. Han, and S. Yang. *Appl Phys Lett* **2004**, *84*, 5434.

[89] M. Deubel, G. Von Freymann, M. Wegener, S. Pereira, K. Busch, and C. M. Soukoulis. *Nat Mater* **2004**, *3*, 444.

[90] M. S. Rill, C. Plet, M. Thiel, I. Staude, G. Von Freymann, S. Linden, and M. Wegener. *Nat Mater* **2008**, *7*, 543.

[91] S. Wong, M. Deubel, F. Pérez-Willard, S. John, G. A. Ozin, M. Wegener, and G. von Freymann. *Adv Mater* **2006**, *18*, 265.

[92] W. Longley and T. McIntosh. *Nature* **1983**, *303*, 612.

[93] T. H. Epps, E. W. Cochran, T. S. Bailey, R. S. Waletzko, C. M. Hardy, and F. S. Bates. *Macromolecules* **2004**, *37*, 8325.

[94] F. H. Schacher, P. a. Rupar, and I. Manners. *Angew Chem Int Ed* **2012**, *51*, 7898.

[95] A. Urbas, R. Sharp, Y. Fink, E. L. Thomas, M. Xenidou, and L. J. Fetters. *Adv Mater* **2000**, *12*, 812.

[96] Y. Kang, J. J. Walish, T. Gorishnyy, and E. L. Thomas. *Nat Mater* **2007**, *6*, 957.

[97] J. Ruokolainen. *Science* **1998**, *280*, 557.

[98] Y. Fink, A. Urbas, M. Bawendi, J. Joannopoulos, and E. Thomas. *IEEE J JLT* **1999**, *17*, 1963.

[99] M. Bockstaller, R. Kolb, and E. L. Thomas. *Adv Mater* **2001**, *13*, 1783.

[100] J. Moon, Y. Xu, Y. Dan, S.-M. Yang, a.T. Johnson, and S. Yang. *Adv Mater* **2007**, *19*, 1510.

[101] V. Z. Chan. *Science* **1999**, *286*, 1716.

[102] V. N. Urade, T.-C. Wei, M. P. Tate, J. D. Kowalski, and H. W. Hillhouse. *Chem Mater* **2007**, *12*, 768.

[103] A. S. Finnemore, M. R. J. Scherer, R. Langford, S. Mahajan, S. Ludwigs, F. C. Meldrum, and U. Steiner. *Adv Mater* **2009**, *21*, 3928.

[104] E. J. W. Crossland, M. Nedelcu, C. Ducati, S. Ludwigs, M. A. Hillmyer, U. Steiner, and H. J. Snaith. *Nano Lett* **2009**, *9*, 2813.

[105] E. J. W. Crossland, M. Kamperman, M. Nedelcu, C. Ducati, U. Wiesner, D.-M. Smilgies, G. E. S. Toombes, M. a. Hillmyer, S. Ludwigs, U. Steiner, and H. J. Snaith. *Nano Lett* **2009**, *9*, 2807.

[106] D. Wei, M. R. J. Scherer, C. Bower, P. Andrew, T. Ryhänen, and U. Steiner. *Nano Lett* **2012**, *12*, 1857.

[107] P. Docampo, M. Stefik, S. Guldin, R. Gunning, N. a. Yufa, N. Cai, P. Wang, U. Steiner, U. Wiesner, and H. J. Snaith. *Adv Energ Mater* **2012**, *2*, 676.

[108] M. R. J. Scherer and U. Steiner. *Nano Lett* **2013**, *13*, 3005.

[109] M. R. J. Scherer, L. Li, P. M. S. Cunha, O. A. Scherman, and U. Steiner. *Adv Mater* **2012**, *24*, 1217.

[110] E. Kim, Y. Vaynzof, A. Sepe, S. Guldin, M. Scherer, P. Cunha, S. V. Roth, and U. Steiner. *Adv Funct Mater* **2014**, *24*, 863.

[111] T. Hashimoto, K. Tsutsumi, and Y. Funaki. *Langmuir* **1997**, *13*, 6869.

[112] I. Vukovic, S. Punzhin, Z. Vukovic, P. Onck, J. T. M. D. Hosson, and G. Brinke. *ACS Nano* **2011**, *5*, 6339.

[113] I. Vukovic, G. ten Brinke, and K. Loos. *Polymer* **2013**, *54*, 2591.

[114] H.-Y. Hsueh, Y.-C. Huang, R.-M. Ho, C.-H. Lai, T. Makida, and H. Hasegawa. *Adv Mater* **2011**, *23*, 3041.

[115] H.-Y. Hsueh, H.-Y. Chen, M.-S. She, C.-K. Chen, R.-M. Ho, S. Gwo, H. Hasegawa, and E. L. Thomas. *Nano Lett* **2010**, *10*, 4994.

[116] D. A. Olson, L. Chen, and M. A. Hillmyer. *Chem Mater* **2008**, *20*, 869.

[117] H.-Y. Hsueh, H.-Y. Chen, Y.-C. Hung, Y.-C. Ling, S. Gwo, and R.-M. Ho. *Adv Mater* **2013**, *25*, 1780.

[118] M. C. Orilall and U. Wiesner. *Chem Soc Rev* **2011**, *40*, 520.

[119] I. Vukovic, T. P. Voortman, D. H. Merino, G. Portale, P. Hiekkataipale, J. Ruokolainen, G. ten Brinke, and K. Loos. *Macromolecules* **2012**, *45*, 3503.

[120] M.-S. She, T.-Y. Lo, and R.-M. Ho. *Macromolecules* **2014**, *47*, 175.

[121] J. P. A. Fairclough, S.-M. Mai, M. W. Matsen, W. Bras, L. Messe, S. C. Turner, A. J. Gleeson, C. Booth, I. W. Hamley, and A. J. Ryan. *J Chem Phys* **2001**, *114*, 5425.

[122] B. J. Dair, A. Avgeropoulos, N. Hadjichristidis, and E. L. Thomas. *J Mater Sci* **2000**, *35*, 5207.

[123] I. Bita, J. K. W. Yang, Y. S. Jung, C. a. Ross, E. L. Thomas, and K. K. Berggren. *Science* **2008**, *321*, 939.

[124] R. Segalman, H. Yokoyama, and E. Kramer. *Adv Mater* **2001**, *13*, 1152.

[125] S. O. Kim, H. H. Solak, M. P. Stoykovich, N. J. Ferrier, J. J. De Pablo, and P. F. Nealey. *Nature* **2003**, *424*, 411.

[126] V. G. Veselago. *Soviet Physics Uspekhi* **1968**, *10*, 509.

[127] V. G. Veselago and E. E. Narimanov. *Nat Mater* **2006**, *5*, 759.

[128] D. Smith, W. Padilla, D. Vier, S. Nemat-Nasser, and S. Schultz. *Phys Rev Lett* **2000**, *84*, 4184.

[129] J. Pendry. *Phys Rev Lett* **2000**, *85*, 3966.

[130] W. Cai and V. Shalaev. *Optical Metamaterials*. Springer, **2010**.

[131] R. Silin. *Radiophys Quantum El* **1972**, *15*, 615.

[132] A. Boltasseva and V. M. Shalaev. *Metamaterials* **2008**, *2*, 1.

[133] J. B. Pendry. *Science* **2004**, *306*, 1353.

[134] W. Zhang, D. Zhang, T. Fan, J. Ding, J. Gu, Q. Guo, and H. Ogawa. *Mater Sci Eng C* **2009**, *29*, 92.

[135] E. Plum, J. Zhou, J. Dong, V. Fedotov, T. Koschny, C. Soukoulis, and N. Zheludev. *Phys Rev*

B **2009**, *79*, 035407.

[136] Z. Li, M. Mutlu, and E. Ozbay. *J Opt* **2013**, *15*, 023001.

[137] V. K. Valev, J. J. Baumberg, C. Sibilia, and T. Verbiest. *Adv Mater* **2013**, *25*, 2517.

[138] S. Vignolini, N. A. Yufa, P. S. Cunha, S. Guldin, I. Rushkin, M. Stefik, K. Hur, U. Wiesner, J. J. Baumberg, and U. Steiner. *Adv Mater* **2012**, *24*, OP23.

[139] S. Salvatore. *Optical Metamaterials by Block Copolymer Self-Assembly (Springer Theses)*. Springer, Berlin, **2014**.

[140] S. Salvatore, A. Demetriadou, S. Vignolini, S. S. Oh, S. Wuestner, N. A. Yufa, M. Stefik, U. Wiesner, J. J. Baumberg, O. Hess, and U. Steiner. *Adv Mater* **2013**, *25*, 2713.

[141] A. Demetriadou, S. S. Oh, S. Wuestner, and O. Hess. *New J Phys* **2012**, *14*, 083032.

[142] S. S. Oh, A. Demetriadou, S. Wuestner, and O. Hess. *Adv Mater* **2013**, *25*, 612.

[143] P. Farah, S. Salvatore, S. Vignolini, A. Demetriadou, O. Hess, U. Steiner, V. Valev, and J. J. Baumberg. *submitted* **2014**, .

[144] K. Hur, Y. Francescato, V. Giannini, S. A. Maier, R. G. Hennig, and U. Wiesner. *Angew Chem Int Ed* **2011**, *50*, 11985.